Fall 2020

Bio-preservation Potential of Sediment in Eberswalde crater, Mars

Cory Hughes
Western Washington University, hughes34@wwu.edu

Bio-preservation Potential of Sediment in Eberswalde crater, Mars

By

Cory M. Hughes

Accepted in Partial Completion
of the Requirements for the Degree
Master of Science

ADVISORY COMMITTEE

Dr. Melissa Rice, Chair

Dr. Charles Barnhart

Dr. Brady Foreman

Dr. Allison Pfeiffer

GRADUATE SCHOOL

David L. Patrick, Dean

Master's Thesis

In presenting this thesis in partial fulfillment of the requirements for a master's degree at Western Washington University, I grant to Western Washington University the non-exclusive royalty-free right to archive, reproduce, distribute, and display the thesis in any and all forms, including electronic format, via any digital library mechanisms maintained by WWU.

I represent and warrant this is my original work, and does not infringe or violate any rights of others. I warrant that I have obtained written permissions from the owner of any third party copyrighted material included in these files.

I acknowledge that I retain ownership rights to the copyright of this work, including but not limited to the right to use all or part of this work in future works, such as articles or books.

Library users are granted permission for individual, research and non-commercial reproduction of this work for educational purposes only. Any further digital posting of this document requires specific permission from the author.

Any copying or publication of this thesis for commercial purposes, or for financial gain, is not allowed without my written permission.

Cory M. Hughes

November 30th, 2020

Bio-preservation Potential of Sediment in Eberswalde crater, Mars

A Thesis
Presented to
The Faculty of
Western Washington University

In Partial Fulfillment
Of the Requirements for the Degree
Master of Science

by
Cory M. Hughes
November 2020

Abstract

Within Eberswalde crater, Mars, is one of the most well-preserved river delta deposits identified within Mars' rock record, and visually traceable from the deposit, is the partially-intact watershed that fed the paleo-lake that once resided within the crater basin. Aqueous alteration minerals, smectite clays and opaline silica, have been previously identified within the deposit, however the origin of those minerals is not well understood. Through analysis of topographic and hyperspectral data, we seek to ascertain the origin and provenance of these minerals to better understand their formative conditions and formation age. We will also assess Eberswalde crater's potential as a site to explore for preserved evidence of past life on planet Mars. Using hyperspectral data to compare the minima positions of particular absorption features (e.g., ~2.3 μm for metal-OH absorptions in smectite clays) from multiple regions, including the river delta deposit, the watershed, the adjacent Northwest Noachis Terra plateau, we test the hypothesis that the smectites found within the Eberswalde crater deposit are fluvial detritus transported there during the Hesperian age (i.e., 3.5-2.0 Ga). We find that the spectra from these three regions are consistent with each other, and most consistent with lab spectra of Fe/Mg smectite clays, namely nontronite and saponite. The similar CRISM signature, and the fluvial relationship between the rocks within the watershed and the preserved putative delta stratigraphy point to a detrital origin for the smectite clays observed within Eberswalde crater. A detrital origin indicates that the clays formed prior to transport during the late Noachian (i.e., 4.0-3.5 Ga), and possibly within the subsurface, which previous studies indicate may have been the time period and location most amenable to the preservation of evidence of past life on Mars. Furthermore, the presence of detrital clays within the deposit indicate that, during the period when a lake existed within Eberswalde crater and a river delta was forming therein (i.e., during the late Hesperian and/or early Amazonian), the lake was ~neutral-pH and a habitable environment. Taken together, these observations indicate that: (1) within Eberswalde crater is a river delta deposit that formed in a habitable environment, (2) that deposit is made up of layers of sediment composed of minerals that formed during the most habitable period in Mars' ancient history, and (3) those minerals formed in an environment thought to be most likely to preserve evidence of past life. Furthermore, this high concentration of high-biosignature preservation features are within a small rover-accessible locale, so Eberswalde crater represents a strong candidate for consideration for future missions exploring Mars for past habitability. And, the similarities between the Eberswalde crater fluvial system and the Jezero crater system make it a compelling site as a standard of comparison for analyses by the upcoming NASA Perseverance rover mission.

Acknowledgements

This work was funded through the Western Washington University Geology Department. Data analyzed was acquired by the CRISM, CTX, HiRISE, and MOLA mission teams. I extend gratitude to all who contributed to the development of those instruments and missions, and to their ongoing work. The inception of the idea for this work does not belong to me, and I owe Sanjeev Gupta, Nancy McKeown, Melissa Rice, and Nicholas Warner gratitude for letting me take over where they left off a few years prior. Several of the techniques and methods employed in this work are outside my skill set, and I relied on numerous collaborators including Charles Barnhart, Timothy Goudge, and Travis Swanson. This work also benefited from discussions with Benjamin Cardenas, Daniel Aylward, Eric Petersen, Daniel Lalich, Racine Swick, and Caleb Fassett. I would not have been able to complete this thesis without the help of my advising committee, Charles Barnhart, Brady Foreman, and Allison Pfeiffer. I want to thank my undergraduate adviser, David Mohrig, for his unrelenting patience with me during my time at UT Austin, and making it possible for me to pursue my passion as a career. I also owe enormous gratitude to my friends and colleagues in the Western Mars Lab whose fervor for science made the time spent working on this thesis fun. Thanks to my friend, Eric Brown, for shooting hoops with me and allowing me to vent. Thanks to Gemma for her constancy when all else is turmoil. My full heart of thanks goes to my parents, Karen and John, whose limits for generosity and compassion have yet to be found, despite my best efforts. Thanks to my brothers, Joel and Andrew, for thinking what I do is cool; their approval means more than they probably recognize. And, thank you, Melissa, for granting me the opportunity to come to Washington to work with you, and for the tremendous kindness and support you have shown me during my time working in your Lab. I am forever grateful to have had the chance.

Table of Contents

List of Tables and Figures

1. Introduction & Background

1.1 Early Mars

Today the mean atmospheric pressure at the surface of Mars is ~0.6 atm, and a mean surface temperature during the day has been shown to be ~200 K (e.g., Schofield et al., 1997). Within this cold and thin atmosphere, liquid water is not thermodynamically stable, and water on present-day Mars is locked in the cryosphere. However, abundant geologic evidence in the form of massive drainage networks (e.g., Barnhart et al., 2009; Hynek and Phillips, 2003), and numerous preserved fluvially-constructed deposits (e.g., Ansan et al., 2011; Dibiase et al., 2013) indicate that at some point in Mars' history its climate was amenable to overland flow. Dating based on crater counts in regions of fluvial incision and valley network formation indicates that most fluvial activity on the surface of Mars happened from ~4 Ga to ~3.5 Ga (Figure 1) with most ceasing by ~2.8 Ga (Fassett and Head, 2008). Observations consistent with pervasive aqueous activity are not limited to stratigraphic or geomorphic expressions; there is also abundant spectrally observed evidence for water-rich conditions early in Mars history in the form of aqueous alteration minerals such as smectite clays, and opaline silica (e.g., Arvidson et al., 2014; Bibring et al., 2006, Sun and Milliken, 2015; Tarnas et al., 2019). The abundant evidence for overland flow and aqueous alteration on or near the surface of Mars does not adequately address the mystery of Mars' ancient climate, however. Fervent debate has characterized the martian scientific community over the past several decades about whether the fluvial activity was the result of a persistently warm and wet climate with attendant precipitation that produced sustained rivers, lakes, and possibly oceans; if the fluvial activity was punctuated and ephemeral being produced by obliquity changes, impact, or volcanically generated heat leading to melting of subsurface and surficial ice; or if the climate was somewhere in between these two end-members. An evidentiary consensus has formed in favor of a predominantly cool climate punctuated by warming events (Wordsworth et al., 2016). However, regardless of the climatic conditions, the idea that Mars had

abundant water on its surface early in its history is well supported by observational evidence and is virtually undisputed in the scientific community.

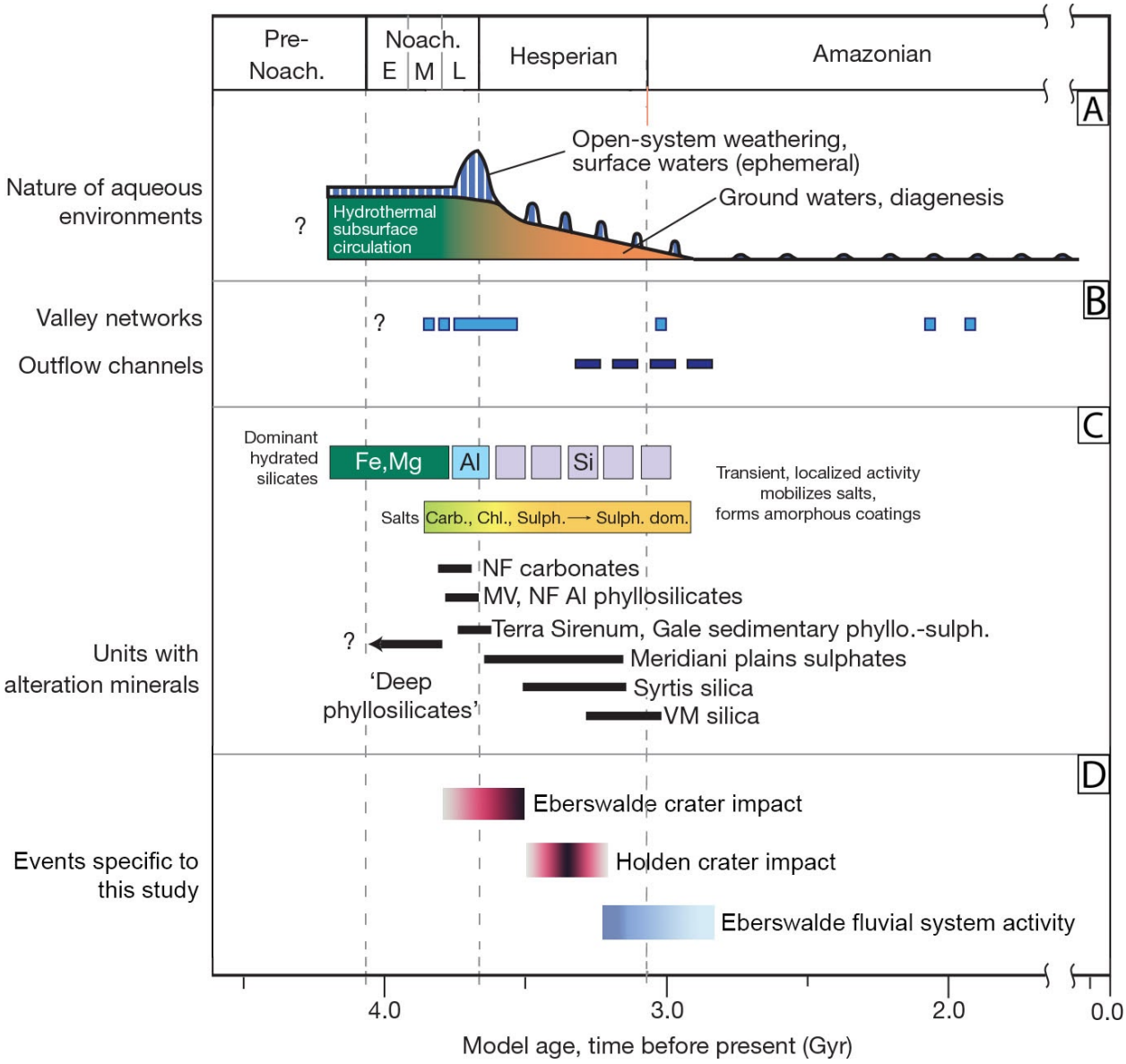

Figure 1: Timeline of relevant processes in Mars geologic history. Modified figure 4 from Ehlmann et al. (2011b), references for ages of events in panels A-C and models therein. Ages of events are approximate and based on relative crater densities and stratigraphic relationships. (A) Changes in aqueous alteration and weathering environments. (B) Timing of valley networks and catastrophic outflow channels. (C) Relative timing for the formation of different alteration products. NF = Nili Fossae; MV = Mawrth; VM = Valles Marineris; Carb. = carbonates; Chl. = chlorites; Sulph.= sulphates. (D) Relative timing for Eberswalde and Holden impact crater events (Rice et al., 2013) and the period of fluvial activity in the Eberswalde crater region (Irwin and Grant, 2011).

1.2 The Search for Evidence of Habitability on Mars

As water is a requisite component of habitable environments (e.g., Cockell et al., 2016; Hoehler, 2007), it is widely hypothesized that Mars may have previously been home to extraterrestrial life. Indeed, potential landing sites with evidence for the presence of liquid water in their past have been favored during the planning of many of NASA's past, current, and future missions to the Red Planet (e.g., Golombek et al., 2012; Grant et al., 2004; Grant et al., 2018), and Eberswalde crater has been a contender as a potential landing site for the last two rover missions (e.g., Golombek et al., 2012; Grant et al., 2018).

Evidence for a variety of potentially habitable ancient martian environments have been identified through analysis of orbital imagery and in-situ robotic science. Hydrothermal systems, subaqueous (i.e., lakes, river deltas), and subsurface (i.e., groundwater aquifers) environments are thought to be among the most likely to have hosted life on Mars' surface (Hays et al., 2011).

Mineralogic and geomorphic evidence for hydrothermal activity is pervasive. Some such instances are the digitate opaline silica deposits found in Gusev crater by NASA's Spirit Rover (Ruff et al., 2020) and the orbital spectroscopy observations in the Nili Fossae region (e.g., Ehlmann et al., 2009; Ehlmann et al., 2010; Ehlmann et al., 2011a; Ehlmann et al., 2013; Mustard et al., 2008) which include spectral signatures consistent with low-grade metamorphic minerals like serpentine and phyllosilicate clays.

Evidence indicates that many of the subaqueous environments that have been identified are ancient crater-confined lakes on the basis of inlet and outlet valleys leading to and from craters (Goudge et al., 2012, Goudge et al., 2015a). However, there is stratigraphic and geomorphic evidence for larger bodies of water in Mars' past (e.g., Adler et al., 2019; Davis, et al., 2019; Dibiase et al., 2013; Hughes et al., 2019) that were not confined by the rim of an impact crater. Ancient martian lakes have garnered considerable attention from the scientific community based, in part, on the presence of well preserved fluvio-deltaic deposits. Such locations include: Gale

crater (landing site of NASA's Curiosity Rover), Jezero crater (future landing site of NASA's Perseverance Rover), and Eberswalde crater.

Widespread evidence for subsurface aqueous environments is also readily observed from orbit in the form of the previously mentioned aqueous alteration minerals, potentially formed in pedogenic conditions (e.g., Le Deit et al., 2012). Notably, some authors suggest that given the uncertainty about Mars' ancient climate, and the possibility that the climate was predominantly cold but with episodic warming events (e.g., Segura et al., 2002), the subsurface aqueous environments may represent the longest duration potentially-habitable environments in Mars' ancient past (Ehlmann et al., 2011b). In a recent analogue study, Azua-Bustos et al. (2020) point to an analogous subsurface biota-rich smectite-bearing layer in the Atacama Desert as an indication of the possibility of subsurface life on ancient Mars.

One such region rife with evidence of past hydrologic activity is the source-to-sink fluvial system at Eberswalde crater. On Mars, source-to-sink sedimentary systems still preserved in the rock record are rare, but most of the Eberswalde crater fluvial system is intact, and can be traced from a deposit within the crater to the highest points of elevation within the putative watershed (Figures 2B and 3A). An ancient but intact source-to-sink system is an excellent geologic setting for investigating the possibility of previously habitable environments. At the upstream end of a fluvial source-to-sink system, we see channelised erosion incising into substrate, carrying sediment from a laterally extensive geographic region through to a distal basin where deposition is focused into a relatively small area. This means that if any region of the system was, at some point in time prior to or during the period of fluvial activity, subject to habitable conditions, evidence from those conditions may be preserved in the deposit.

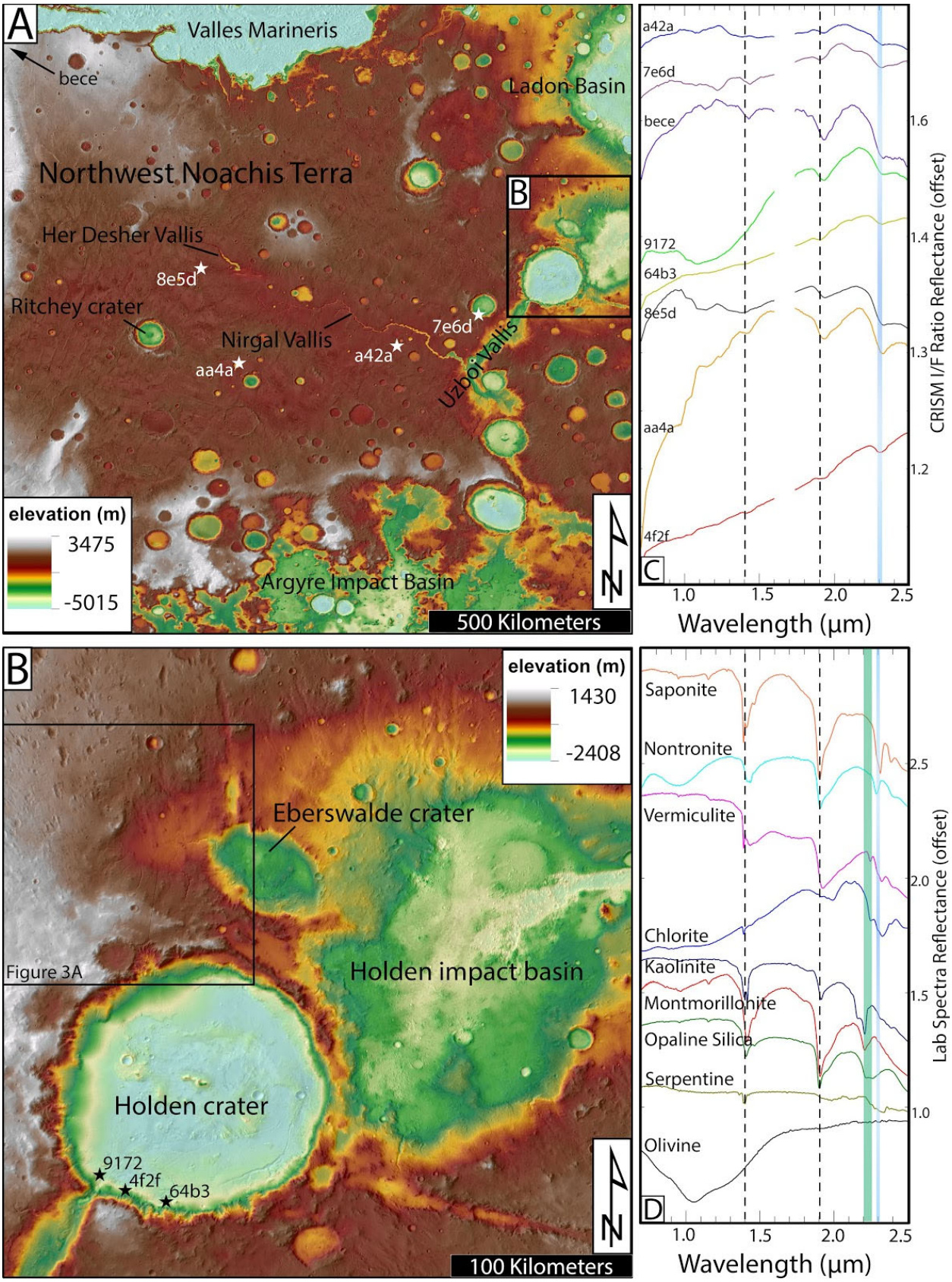
A
Valles Marineris
bece
Ladon Basin
Northwest Noachis Terra
B
Her Desher Vallis
8e5d
Ritchey crater
Nirgal Vallis
7e6d
a42a
aa4a
Uzboi Vallis
elevation (m)
3475
-5015
Argyre Impact Basin
500 Kilometers
a42a
7e6d
bece
9172
64b3
8e5d
aa4a
4f2f
C
1.0
1.5
2.0
2.5
Wavelength (μm)
CRISM I/F Ratio Reflectance (offset)
1.6
1.4
1.3
1.2
B
elevation (m)
1430
-2408
Eberswalde crater
Figure 3A
Holden impact basin
Holden crater
9172
4f2f
64b3
100 Kilometers
Saponite
Nontronite
Vermiculite
Chlorite
Kaolinite
Montmorillonite
Opaline Silica
Serpentine
Olivine
D
1.0
1.5
2.0
2.5
Wavelength (μm)
Lab Spectra Reflectance (offset)
2.5
2.0
1.5
1.0

Figure 2: Regional and local context of the study area accompanied by ratioed spectra of "Plateau Phyllosilicates" and example laboratory spectra. (A) Regional context of the study area shown with daytime Thermal Emission Imaging System (THEMIS) data (Christensen et al., 2004) with Mars Orbiter Laser Altimeter (MOLA) point shot elevation data (Smith et al., 2001) overlain. Notable geographic features labeled and indicated accordingly. Approximate locations of extracted CRISM spectra from the northwest Noachis Terra plateau labeled with stars and the final four characters of their observation ID (full IDs are listed in Table 1). (B) Same as (A) but for the local context of the Eberswalde crater study area. (C) CRISM I/F ratioed spectra from Noachis Terra and Holden crater which are offset for clarity. Spectra are smoothed using a moving box-car average with the two closest data points on either side of a bandpass. Dashed vertical lines correspond to the ~1.4 μm and ~1.9 μm water overtone absorption features for hydrated minerals. Blue vertical bar spans the 2.29 - 2.31 μm metal-OH absorption features for Mg/Fe smectite clays, saponite and nontronite. Green vertical bar spans the 2.21 - 2.26 μm Si-OH absorption feature for opaline silica. (D) Example laboratory spectra of relevant minerals from the USGS spectral library (Kokaly et al., 2017). Dashed vertical lines and vertical bars are the same as for (C).

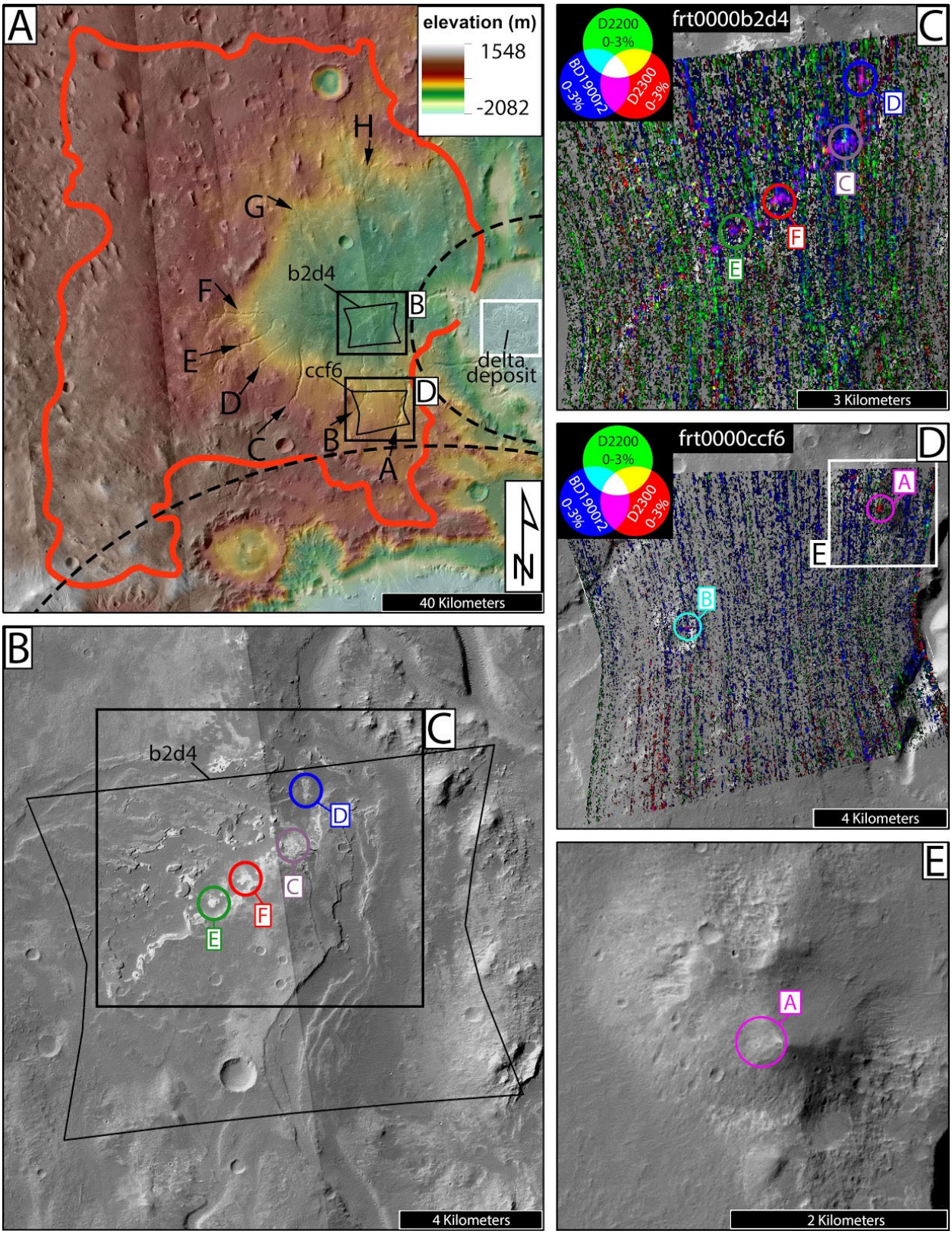

Figure 3: Local context of Eberswalde crater fluvial system and watershed. North is up in all panels. (A) Eberswalde crater approximate watershed from Mangold et al. (2012) outlined in red

shown with a mosaic of day-time THEMIS and CTX images B06_011898_1558, J02_045550_1560, B21_017911_1559, B21_017700_1557, B02_010619_1561, G02_019111_1548, B22_018333_1548, and B02_010263_1557. overlaid by MOLA point shot elevation data. Black dashed lines correspond to radial distances of 20 km and 30 km from the Eberswalde and Holden crater rims respectively; these dashed lines correspond to the back vertical lines in Figures 10 and 11 - beyond those distances is the region most dissected by the tributaries of the Eberswalde watershed (i.e., volumetrically, the majority of the sediment deposited in the delta would have been sourced from this region). Letters indicate valleys measured for incision depth (results reported in Table 4) with the first measurement on each valley being the furthest upstream with subsequent measurements spaced ~2 km apart down stream. Main delta deposit labeled and outlined with white box which roughly corresponds to Figure 4A. CRISM observation bowtie-shaped footprints outlined in black labeled with the last four letters of the observation ID (full IDs are listed in Table 1). (B) Inter-watershed basin region with fluvial sedimentary deposits shown with CTX images B02_010263_1557 and B22_018333_1548. Bowtie outline indicates the footprint of CRISM observation frt0000b2d4 shown in (C). Colored circles and letters correspond to ROIs with ratioed spectra shown in Figure 9A. (C) Roughly the same region as (B) with CRISM RGB summary parameter map PHY (Viviano-Beck et al., 2014) from CRISM observation frt0000b2d4 overlain on the same CTX images as (B). Concentrations of red (D2300 parameter, Table 2) and magenta (D2300 + BD1900r2 parameters) colored pixels indicate regions with possible exposures of Fe/Mg smectite clays. Colored circles and letters correspond to ROIs with ratioed spectra shown in Figure 9A. (D) Upstream portion within Eberswalde crater watershed with CRISM RGB summary parameter map PHY indicating possible exposures of hydrated phyllosilicates from CRISM observation frt0000ccf6 overlain on the same CTX image as (B) and (C). Colored circles and letters correspond to ROIs with ratioed spectra shown in Figure 9A. (E) Same CTX images as other panels show putative mega-breccia block from Holden crater impact (Mangold et al., 2012) with spectra consistent with Fe/Mg phyllosilicate clays. Colored circle and letter correspond to ROI with its ratioed spectrum shown in Figure 9A.

1.3 Eberswalde Crater

Eberswalde crater is a ~70 km diameter oblate depression centered at -23.59º N, 33.17º W that formed from an impact in the late Noachian (Pondrelli et al., 2011) or the early Hesperian (Rice et al., 2013a). It is located NNE of the larger and younger Holden Crater which formed in the early to late Hesperian (Rice et al., 2013a) (Figure 2B). Megabreccia is visible within the Eberswalde crater floor material, which is interpreted as Holden impact breccia (Rice et al., 2013a), constraining the temporal order of impacts with the Eberswalde impact taking place first. The source of Eberswalde's oblate shape is not well understood. It could be the result of a singular oblique impact, or perhaps two contemporaneous impacts with subsequent erosion removing the shared crater rim (Moore et al., 2003; Irwin et al., 2015). Also plausible is that the crater was originally symmetrical in shape, but has since been deformed by younger impacts (e.g., the Holden crater impact) and post-impact geomorphic processes (Rice et al., 2013a).

Within Eberswalde crater is one of the most pristinely preserved branching-fluvial complexes yet identified on the surface of Mars (Figure 3B and Figure 4A), along with several other smaller fan-shaped fluvial deposits (e.g., Rice et al., 2011; Goddard et al., 2014). The main fan-shaped branching network of topographically-inverted channels (Figure 3B) is widely considered to be deltaic in origin (Malin and Edgett, 2003; Moore et al., 2003; Battacharya et al., 2005; Lewis and Aharonson, 2006; Wood, 2006; Pondrelli et al., 2008, 2011; Rice et al., 2011, 2013a; Mangold et al., 2012; Irwin et al., 2015), or an alluvial fan (Jerolmack et al., 2004). As a result of this uncertainty about the depositional setting and difficulties associated with interpreting hydrogeologic history from orbit (e.g., Hayden et al., 2019), a wide range of estimates exist for the duration of the fluvial system. Most recently, Irwin et al. (2015) reviewed the published hypotheses and evidence presented by previous studies and suggested a range from 70,000 years to 150,000 years assuming climatic conditions were somewhere between the warm and wet and the cold and dry scenarios. All formation periods are minimum estimates on the basis of several assumptions as stated by Irwin et al. (2015): (1) that the water flowing into the crater was continuously sediment laden, (2) that the water flowing into the crater came only from the channels that formed the deltaic deposit, and (3) that all sediment delivered to the crater is captured within the current extent of the deposit, which discounts erosion and sediment that may have been carried and deposited elsewhere within the crater. There is also the matter of intermittency associated with factors like seasonal or climatic variations in precipitation and runoff, which could significantly lengthen the formation time (e.g., Lapotre and Ielpi et al., 2020). Nevertheless, the minimum estimates for the longevity of this fluvial system point to a significant volume of liquid water present in the Eberswalde crater lake at some point in Mars' early history. Supporting the hypothesis of a non-ephemeral lake, Pondrelli et al. (2011) present evidence for changes in base-level in the form of several differently aged depositional lobes.

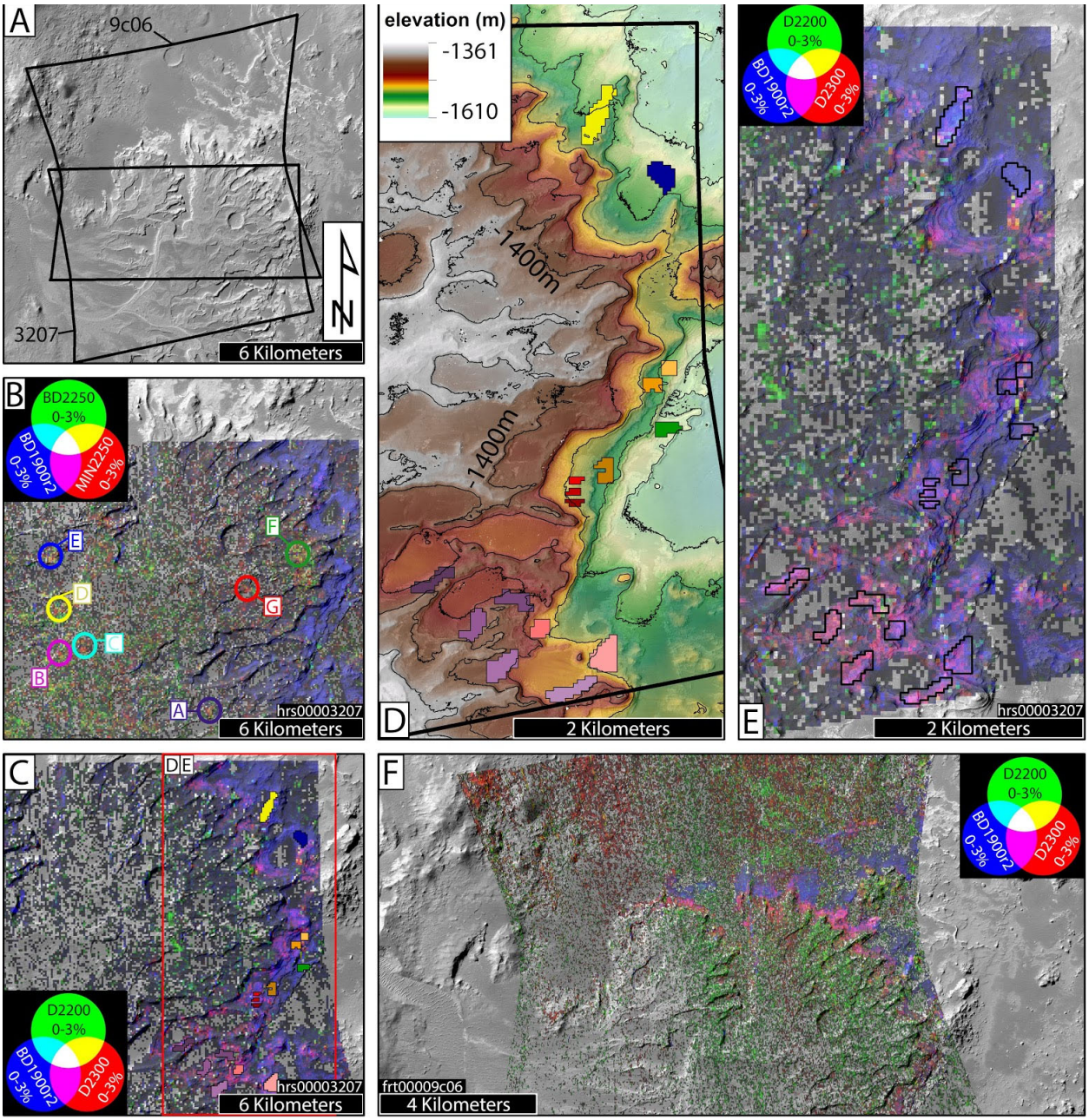

Figure 4: CRISM MTRDR coverage and investigation of the pristine putative deltaic deposit within Eberswalde crater. North is up for all panels. (A) CTX image B21_017911_1559 with outlines indicating the extent of each MTRDR footprint over the main delta deposit in Eberswalde crater. The footprints are labeled with the final four digits of the observation ID. (B) Same CTX image as (B) overlain with CRISM MTRDR hrs00003207 summary parameter map HYS (Viviano-Beck et al., 2014) indicating possible exposures of opaline silica. Note the strong hydration signature (BD1900r2, blue pixels, Table 2) along the erosional front of the deposit (right side of the image) and that the green (BD2250), red (MIN2250), and yellow (BD2250 + MIN2250) pixels are exclusively on top of the deposit. Colored circles and letters correspond to ROIs with ratioed spectra shown in Figure 9A. (C) Same as (B) but with summary parameter map PHY indicating possible exposures of hydrated phyllosilicates. Concentrations of red (D2300 parameter, Table 2) and magenta (D2300 + BD1900r2 parameters) colored pixels indicate regions with possible exposures of Fe/Mg smectite clays. Note the concentration of red, magenta, and blue pixels along

the erosional front of the deposit (right side of the image), indicating possible Fe/Mg smectite clays within the exposed river delta stratigraphy. Red box around the erosional front of the deposit indicates the region shown in panels (D) and (E). Colored polygons correspond to location and extent of ROIs drawn to analyze the spectral characteristics of the erosional front of the deposit; spectra shown in Figure 9B. (D) HiRISE image pair ESP_047119_1560+ESP_047185_1560 stereo-derived DEM overlain on an orthophoto generated from the same pair. The contour interval is 20 m; -1400 m contour is labeled. Thick black line indicates the extent of CRISM MTRDR hrs00003207. Colored polygons correspond to location and extent of ROIs drawn to analyze the spectral characteristics of the erosional front of the deposit; spectra shown in Figure 9B. (E) Same HiRISE stereo-derived orthophoto as (D), but overlain with summary parameter map PHY indicated possible exposures of hydrated phyllosilicates. Black polygons correspond to location and extent of ROIs drawn to analyze the spectral characteristics of the erosional front of the deposit. (F) Same CTX image as (A), (B), and (C) with CRISM MTRDR observation frt00009c06 summary parameter map PHY overlain indicating possible exposures of hydrated phyllosilicates. Note the concentration of red, magenta, and blue pixels along the erosional front of the deposit (middle of the image), indicating possible Fe/Mg smectite clays within the exposed river delta stratigraphy, consistent with hrs00003207 from panels (C) and (E).

Previous estimates of the scale of the contributing drainage basin or watershed range from 4000 km^2 to 17,000 km^2 (Malin and Edgett, 2003; Moore et al., 2003; Battacharya et al., 2005; Pondrelli et al., 2008; Mangold et al., 2012; Irwin et al., 2015;). In Figure 3A we show the rough extent of the watershed as calculated using a hydraulic analysis system, DNR hydromod (Loesch, 2001) by Mangold et al. (2012) outlined in red, which extends far beyond the furthest upstream portions of the visibly identifiable erosional valleys. This disparity between the current lateral extent of valley incision and the much larger calculated extent may be explained by denudation and/or infilling the many years since the last period of fluvial activity. Malin and Edgett (2003) and Moore et al. (2003) suggest that the erosional valleys of the watershed are incising into a Noachian-aged, thoroughly-eroded crater referred to informally as the Holden impact basin (Figure 3A). One consideration that has been missed in the prior peer-reviewed literature is that these valleys would also likely be incising into some thickness of remnant ejecta from both the Eberswalde and Holden craters. It remains unclear whether or not the erosional channels of the Eberswalde watershed system incise deeply enough to sample the Noachian terrain beneath the crater ejecta layers. If the channels did erode deeply enough to incise into the Noachian terrain, they may have carried high-biopreservation potential sediment to the Eberswalde deposit.

Milliken and Bish (2010) and Poulet et al. (2014) presented evidence for broad exposure of iron and magnesium smectites, particularly saponite and nontronite, exposed on the erosional front of the putatively deltaic deposit within Eberswalde crater (Figure 3C). Milliken and Bish (2010) suggested that these clays are detrital based on the identification of spectra consistent with a similar assemblage of phyllosilicates in the crater rim of the adjacent Holden crater. However, the region of the Holden crater rim analyzed by Milliken and Bish (2010) is not sampled by the network of erosional valleys that feed the Eberswalde deposit. In a conference abstract, McKeown et al. (2013) presented reflectance spectra from within the Eberswalde watershed that are consistent with the clays observed in the deposit. However, this observation was not presented in a peer-reviewed publication, and the presented results are from only one of several spectral datasets sampling the watershed's extent. Further analysis of other locations within the watershed is needed to confirm these results.

In addition to the presence of altered clay phases, Poulet et al. (2014) identified spectral trends on the delta top that are consistent with opaline silica. They argued that the presence of opaline silica is indicative of an authigenic origin for the clays found within the delta. This period of authigenic formation is suggested to have been coeval with the period of deposition that formed the delta, or during a post-depositional period of sediment dehydration, because opaline silica is unstable when interacting with water subsequent to its initial precipitation. Given the opposing interpretations for the formation of the clay minerals observed within the Eberswalde deposit, the timing and location of the aqueous alteration remains underdetermined. More specifically, it is unclear whether these clays formed by aqueous alteration in-situ (i.e., authigenically within the crater), or if they formed by aqueous alteration prior to fluvial transport and were therefore deposited as fluvial detritus in the crater basin.

1.4 Regional Context for Eberswalde Crater

The Eberswalde and Holden impact craters are located within an early Noachian-aged crater informally referred to as the Holden impact basin (Figures 2A and 2B)(Malin and Edgett, 2003; Moore et al., 2003; Irwin et al., 2015). The Holden impact basin is a part of a larger geographic feature referred to as the Uzboi-Ladon-Morava (ULM) system which is a roughly 3,000 km long network of valley-connected impact craters and basins that links Bond Crater, which is just ~100 km north the Argyre Impact Basin in the southern highlands, with Chryse Planitia in the northern lowlands (Figure 2A). Observational evidence indicates that the ULM system formed through a combination of quotidian fluvial and catastrophic flooding events spanning the Noachian to late Hesperian (Grant and Parker, 2002). The ULM valley system is located southeast Valles Marineris and northeast of the Argyre impact basin. Between these three topographically-low features a broad plateau exists, which is informally referred to as “northwest Noachis Terra” (NT) (e.g., Buczkowski et al., 2010a) (Figure 2A). NT is populated by numerous well retained craters and valley networks including Ritchey crater, Nirgal Vallis, and Her Desher Vallis (Figure 2A). Buczkowski et al. (2010a) presented spectral evidence for laterally-extensive and northward-dipping, iron/magnesium and aluminum phyllosilicate-bearing strata that span the entirety of the NT plateau. In a broad study of 90 orbital-derived spectroscopic observations, Le Deit et al. (2012) confirmed the observations made by Buczkowski et al. (2010a), referring to the regionally-extensive strata as the “Plateau Phyllosilicates.” Le Diet et al. (2012) demonstrated that the "Plateau Phyllosilicates” cover a minimum of ~197,000 km^2 and suggested that these clays formed through pegogenic processes, citing the transition from aluminum rich clay layers above and iron and magnesium rich layers below as evidence for soil horizons. In a later abstract, Buczkowski et al. (2013) presented spectroscopic observations from Nigral Vallis and Her Desher Vallis consistent with multiple layers of iron/magnesium and aluminum rich clays, in addition to those presented by Le Deit et al. (2012). And, based on the geomorphology of the Nigral Vallis and Her Desher Vallis, Buczkowski et al. (2014) suggested that the “Plateau Phyllosilicates”, and the

additional layers observed by Buczkowski et al. (2013), formed via groundwater interactions with the substrate rather than top-down weathering such as pedogenesis. Weitz et al. (2018) found a similar clay bearing layer in the Ladon Valles region, and Wilson et al. (2018) found spectral evidence in the Uzboi Vallis deposits that are consistent with phyllosilicate clays. A broad study of spectroscopic observations of exposed layers within cliff sides of the Argyre Basin ring structure revealed similar phyllosilicate bearing strata (Buczkowski et al., 2010b). Regardless of the formation mechanism, there is abundant evidence of a laterally extensive layer or layers of Noachian-aged phyllosilicate clays in NT consistent with the formation time suggested by Ehlmann et al. (2011) (Figure 1), and Eberswalde Crater sits on the eastern edge of this region (Figure 2A).

1.5 Remaining Questions

If the erosional valley network of the Eberswalde crater fluvial system does incise deeply through the layers of the Holden and Eberswalde impact ejecta into Noachian substrate, it is possible that the fluvial network carried material from the Noachian-aged “Plateau Phyllosilicates” observed by Le Deit et al. (2012) and the additional layers identified by Buczkowski et al. (2013). If that is the case, it is plausible that the rivers that fed the Eberswalde Crater lake carried clay-rich sediment from strata that formed via pedogenic or groundwater alteration from the watershed and deposited it within the putative delta, in turn, concentrating high biosignature potential sediment from a broad geographic region in a confined, rover-accessible area (e.g., Ehlmann et al., 2011) (Figure 1).

Additionally, how the timing of the formation of the clays found within the Eberswalde deposit relates to the planet-wide aqueous alteration timeline put forward by Ehlmann et al. (2011) presents an interesting unresolved problem, particularly considering that the period of predominant Fe/Mg clay formation (Noachian) substantially predates the putative period of fluvial activity at Eberswalde crater, which is late Hesperian or younger (Mangold et al., 2012). It is still unclear whether or not the clays formed within the watershed region prior to fluvial activity, or if

the clays formed subsequent to fluvial deposition within the crater basin. If results indicate that the clays are indeed detrital, as Milliken and Bish (2010) suggest, then it is plausible that the period of alteration occurred during the Noachian in accordance with the findings of Ehlmann et al. (2011). However, if the results indicate that the clays are authigenic, as Poulet et al. (2014) suggest, then the clays within the deposit at Eberswalde crater are the result of a period of aqueous alteration that occurred much later in Mars' history than the Noachian. Therefore, further analyses of Eberswalde crater could offer new insight for the Mars science community's understanding of Mars geologic and hydrologic history.

In this study, we test multiple hypotheses about the origins of the clays observed in primary the Eberswalde crater deposit. We test for evidence of spectrally-similar clays in the watershed; such a presence would point to a detrital origin for the clays within the crater. We also test for spectral similarities between the Eberswalde clays and "Plateau Phyllosilicates" to further constrain potential sources. And, we test whether the erosional valleys in the Eberswalde fluvial watershed incised through the Holden and Eberswalde impact ejecta blankets by modeling their and measuring valley depth. We also consider impact-induced excavation of buried clay-rich sediment as a method for emplacing smectite clay minerals within the watershed. The results of these tests will shed new understanding about the provenance of the Eberswalde fluvial system, constrain the likelihood that the clay-bearing deltaic deposit in Eberswalde crater preserves biosignature rich sediment from the Noachian, and given the similarities between Eberswalde crater and Jezero crater (i.e., the presence of an intact source-to-sink fluvial system that terminates with a putatively deltaic deposit), a better understanding of the Eberswalde system may provide a useful martian analogue for the NASA Perseverance Rover landing site.

2. Methods

2.1 CRISM Data Processing and Analysis

The Compact Reconnaissance Imaging Spectrometer for Mars (CRISM) is a hyperspectral instrument aboard the Mars Reconnaissance Orbiter (MRO) with data available in a variety of products that range from untargeted, low spatial resolution, regional mapping observations (~200 m^2/pixel) to fully targeted, high spatial resolution, locale characterization observations (~18 m^2/pixel). In this study we make use of smaller footprint, high spatial resolution products called full resolution targeted (FRT) and half resolution long (HRL), with spatial resolutions of ~18 m^2/pixel and ~36 m^2/pixel respectively. CRISM has 544 band passes that cover a spectral range from 0.362 μm to 3.92 μm at intervals of 0.00655 μm, and has an instrumental error of ~1% (Murchie et al., 2007). For investigations focused on aqueous alteration minerals the spectral range of interest is the visual to near-infrared (VNIR) which is from ~0.8 μm to ~2.5 μm. A full list of the CRISM observations analyzed in this study can be found in Table 1.

Table 1: List of CRISM Observations analyzed in this study.

Observation ID	Acquisition Date	Observation Type	Location	Clays?
hrs00003207	2006-11-23	CRISM - MTRDR	Eberswalde crater - primary deposit in west	Yes
frt00009c06	2008-02-02	CRISM - MTRDR	Eberswalde crater - primary deposit in west	Possibly
frt00003eeb	2007-01-17	CRISM - MTRDR	Eberswalde crater - northeast	No
frt00008038	2007-10-03	CRISM - MTRDR	Eberswalde crater - central	No
frt0000524a	2007-04-04	CRISM - MTRDR	Outside Eberswalde crater - north	No
frt0000b548	2008-07-02	CRISM - MTRDR	Eberswalde crater - north central	No
frt0000aade	2008-05-02	CRISM - MTRDR	Eberswalde crater - central	No
frt0000a30c	2008-03-01	CRISM - MTRDR	Eberswalde crater - central	No
frt0000a8d1	2008-04-20	CRISM - TRDR	Eberswalde watershed - north	No
frt0000b2d4	2008-06-21	CRISM - TRDR	Eberswalde watershed - central	Yes
frt0000ccf6	2008-10-04	CRISM - TRDR	Eberswalde watershed - south	Yes
frt0000aa4a	2008-04-28	CRISM - MTRDR	NT - Small crater east of Ritchey crater	Yes

hrl0000bece	2008-08-05	CRISM - MTRDR	NT - Coprates Chasma	Yes
frt00008e5d	2007-12-22	CRISM - MTRDR	NT - Small craters southwest of Her Desher Vallis	Yes
hrl00007e6d	2007-09-27	CRISM - MTRDR	NT - Crater east of Holden crater	Yes
hrl0000a42a	2008-03-05	CRISM - MTRDR	NT - Small crater south of Nigral Vallis	Yes
hrl0000599a	2007-04-25	CRISM - MTRDR	NT - Crater south of Nigral Vallis	No
frt0000abb5	2008-05-07	CRISM - MTRDR	Uzboi Vallis	No
frt00009172	2007-12-30	CRISM - MTRDR	Holden crater - just inside southern inlet - east	Yes
hrl0000661e	2007-06-25	CRISM - MTRDR	Holden crater - just inside southern inlet - west	No
frt000064b3	2007-06-20	CRISM - MTRDR	Holden crater - south central along rim	Yes
frt00006246	2007-06-09	CRISM - MTRDR	Holden crater - south central along rim	No
frt00004f2f	2007-03-24	CRISM - MTRDR	Holden crater - south central along rim	Yes
frt0000474a	2007-02-24	CRISM - MTRDR	Holden crater - southwest central	No

To make scientific use of CRISM data we need to know the reflectance value at the relevant wavelengths (e.g., H_2O and metal-OH produce absorption features at ~1.9 μm and ~2.3 μm respectively, Clark et al., 1990) (Figure 2D). However, CRISM's detectors measure irradiance (light flux density), which is a value that decreases according to the inverse of the square of the distance from the object emitting/reflecting the light, and is not equivalent to a reflectance value. Given that we know the elevation of an imaged martian surface from the Mars Orbiter Laser Altimeter (MOLA) data (Smith et al., 2001) and we know the position of MRO in space (i.e., we know the distance from our instrument to the surface), we can calculate the value of the radiance of the target (L), which is the absolute magnitude of light being emitted/reflected from the surface without respect to distance. Knowing the incoming irradiance from the Sun (F), we can then calculate the reflectance of the target with the following equation:

$$\text{Reflectance} = L/\pi F = I/F \qquad \text{[Eqn. 1]}$$

This correction, commonly referred to as correcting for I/F, does not account for the angle of the incoming light, however, so another correction must be made by dividing reflectance by the cosine of the incidence angle which varies depending on the time of day and the latitude of the target. In most cases, we must also account for emission, absorption, and scattering of light as it interacts with gasses and aerosols in Mars' atmosphere. This is done using a 'volcano scan' which calculates a ratioed spectrum from a spectrum taken at the base of Olympus Mons and one at the summit (i.e., spectrum from a thicker Mars atmosphere divided by a spectrum from a thin or absent atmosphere, McGuire et al., 2009). This ratioed spectrum is then scaled to account for each observation of interest. For select FRT and HRL observations, some preprocessing has been performed by the CRISM team at Johns Hopkins University Applied Physics Laboratory (JHU-APL), including correcting for I/F, map projecting, correcting for spectral smile, and removing atmospheric noise via the volcano scan. These preprocessed observations are called Map Projected Target Reduced Data Records (MTRDRs) (Seelos et al., 2016). Other FRTs, namely Target Reduced Data Records (TRDRs) require processing and correction prior to analysis following the steps outlined above and described in detail by Murchie et al. (2006).

To study the provenance of the Eberswalde fluvial system, we started by thoroughly characterizing the spectral trends within the deposit. Regions of interest (ROIs) were drawn using polygons in the geo-spatial analysis software ENVI (examples of ROIs are shown in Figures 4C, 4D, and 4E). ROIs were used to establish a set of raster grid cells containing spectral values used to calculate the mean spectra for all cells within the ROI. Each ROI covered multiple pixels (>5 pixels) to reduce the effects of instrumental and environmental noise. To ensure fidelity from measurements at multiple scales, larger ROIs were also drawn over areas that covered regions encapsulating several smaller ROIs, and the results were largely the same. With smaller ROIs we gained the ability to test for variability along stratigraphic exposures at the delta front (e.g., Figures 4D and 4E) at the cost of statistical noise in the resulting spectra (e.g., Milliken and Bish 2010).

Given that Mars is inherently dusty, we must account for error associated with dust cover on surfaces of interest. To minimize the effect of dust within extracted spectra we divided each ROI spectrum by the spectrum of an ROI drawn around a spectrally bland region which resulted in a useful 'ratioed spectra' (e.g., Ackiss et al., 2018; Horgan et al., 2020). Bland ROIs were selected to be within the same columns of the CRISM detector grid as the particular ROI that it is divided into to reduce detector-column related instrumental noise. This typically required a unique bland ROI for each measurement ROI. In the case of MTRDRs this is not an issue, and bland ROIs from MTRDR observations can be anywhere within the observation which permits a single bland ROI for multiple measurement ROIs (e.g., Horgan et al., 2020; Seelos et al., 2016). This method allowed us to spectrally characterise the mineralogy and assess the relationships of the rocks in the deposit stratigraphy, the Eberswalde watershed, and regions of NT by comparing our CRISM spectral results to laboratory spectra (e.g., Figure 2D).

For comparison to CRISM data, spectra of laboratory minerals (i.e., chlorite, kaolinite, montmorillonite, nontronite, saponite, vermiculite, saponite, and olivine) were chosen on the basis of spectral trends similar to those we recognized in our CRISM spectra, and, for some, as a representative set of aqueous alteration minerals from other CRISM studies in the peer-reviewed literature. Laboratory sample spectra were retrieved from the USGS Spectral Library (Kokaly et al., 2017) (Figure 2D).

To aid with ROI selection, we made use of summary parameter maps (e.g., Viviano-Beck et al., 2014), which are observation-wide raster products that display spatial trends associated absorption features of interest. We found the parameter map, PHY (e.g., Figure 3C, Viviano-Beck et al., 2014), to be most useful. It maps spectral features pertinent to the search for evidence of phyllosilicate minerals, including the ~2.3 μm feature associated with metal-OH bonds in hydrated clay minerals (D2300, Table 2), the ~2.2 μm absorption feature associated with Al-OH in aluminosilicates and Si-OH bonds in hydrated silica minerals and mineraloids (D2200, Table 2), and the ~1.9 μm H_20 overtone (BD1900r2, Table 2). We also made use of the hydrated silica

summary parameter map, HYS, which maps features such as the broad ~2.21 - 2.26 μm absorption feature associated with opaline silica deposits (MIN2250, Table 2), the band depth at ~2.25 μm (BD2250, Table 2), and the ~1.9 μm H_20 overtone (BD1900r2, Table 2).

Table 2: List of summary parameters used. Full descriptions with formulations can be found in Viviano-Beck et al. (2014).

Parameter	Spectral Feature Description	Rationale
D2300	2.3 μm dropoff	Hydroxylated Fe,Mg silicates strongly > 0
D2200	2.2 μm dropoff	Al-OH minerals
BD1900r2	1.9 μm H_20 band depth	H_20
MIN2250	2.21 μm Si-OH band depth and 2.26 μm H-bound Si-OH band depth	Opal
BD2250	2.25 μm broad Al-OH and Si-OH band depth	Opal and other Al-OH minerals

To compare the mineralogy of the different geographic regions (i.e., the Eberswalde crater deposit, the Eberswalde crater fluvial watershed, and the adjacent NT and Holden crater clays) we compared the shape of extracted spectra and the wavelengths of any absorption features present along the curve. Absorption features are represented by a decrease in the reflectance value at a specific wavelength (e.g., 2.29 μm for nontronite) or across a range of wavelengths (e.g., 2.21 - 2.26 μm for opaline silica). More specifically, based on results in published literature (Miliken and Bish, 2010; Poulet et al., 2014), we expected to find Fe and Mg clays and opaline silica within the Eberswalde crater deposit. Fe and Mg clays have absorption features at ~2.29 μm and 2.32 μm respectively, and opaline silica has a broad absorption feature that spans ~2.21 μm to ~2.26 μm (e.g., Smith et al., 2013).

We also calculated and plotted pertinent spectral parameters from continuum-removed and smoothed spectra (e.g., Figure 5). A spectrum is smoothed using a moving boxcar-average method with a boxcar width of five data points. A continuum is defined as a curve fit along top of a spectrum using straight line segments to connect local reflectance maxima. The entire spectrum

is then divided by this continuum to provide a baseline for measurements and comparison to other spectra. For a more detailed description of the continuum removal process refer to Clark and Roush (1984). The three pertinent spectral parameters used are: (1) the precise minima position of the ~2.2 - 2.4 μm absorption feature, (2) the precise minima position of the ~1.9 μm absorption feature, and (3) the full-width half-maximum (FWHM) value centered about the minima position of the ~2.2 - 2.4 μm absorption feature. As stated above, the minima position of the ~2.2 - 2.4 μm absorption feature is used to determine which mineral phase is most consistent a given spectrum extracted from the CRISM data. The precise minimum position is calculated by hand selecting two shoulder positions on either side of an absorption feature, and then finding the wavelength that corresponds to the lowest reflectance value between those two shoulder positions (e.g., Figure 5). FWHM values are calculated by first calculating the band depth of a particular feature. Band depth is calculated as the difference between mean reflectance of both shoulders on the smoothed and continuum-removed spectrum and the local minimum reflectance in the absorption feature of interest. The width at the half-band depth is approximated by projecting a horizontal line from the half-band depth reflectance value directly above the minimum wavelength position to find wavelength intercepts on the left and right flanks of the absorption feature. The distance between these two intercepts (i.e., the difference between two wavelength values at the horizontal line's intersections with the smoothed and continuum removed spectrum) is the full-width at half maximum value (e.g., Figure 5). FWHM values are useful for assessing how closely a spectrum represents a pure phase of a particular mineral. A spectrum extracted from a region of Mars' surface that has several minerals with overlapping bands that have slightly offset minima and shoulder positions is expected to have broader absorption features and therefore larger FWHM values.

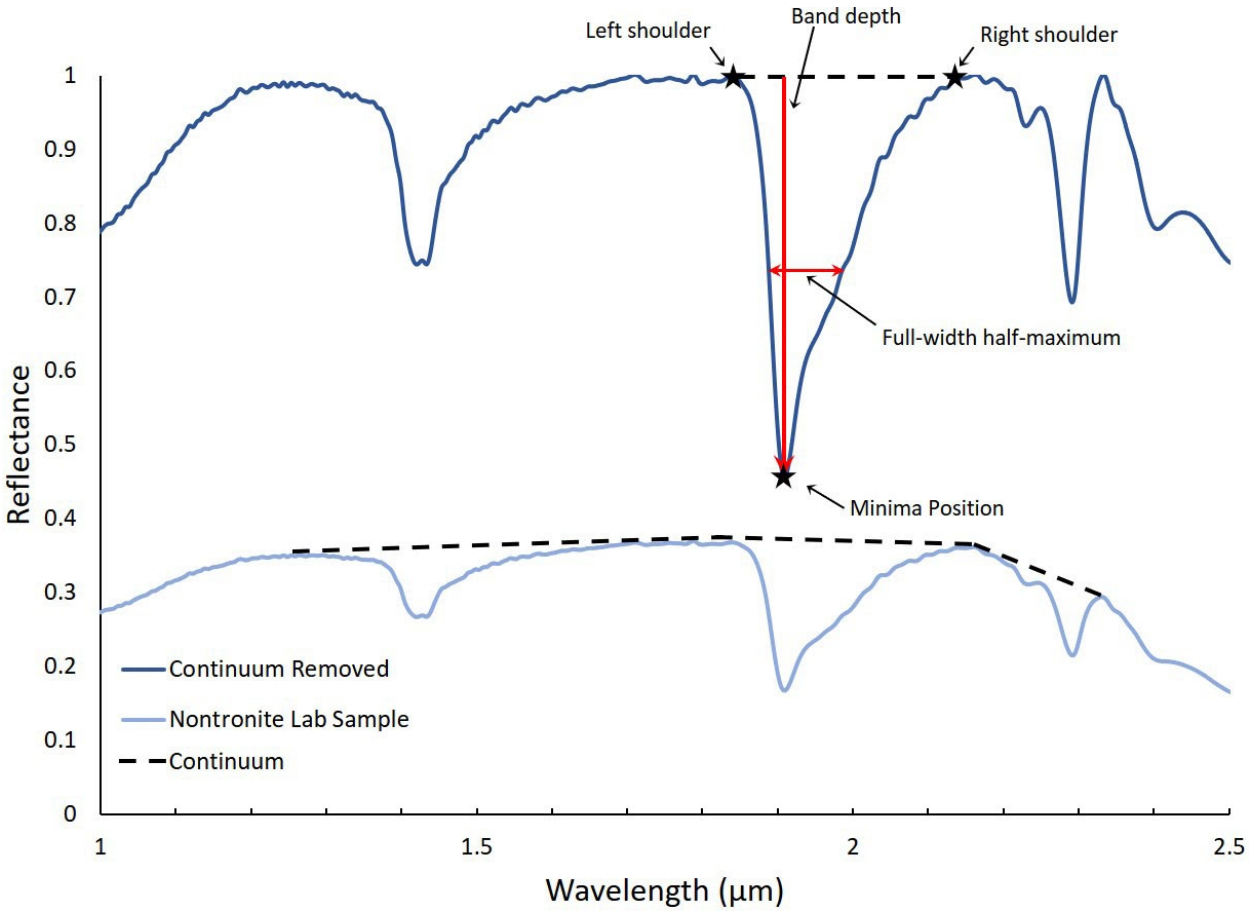

Figure 5: Graphic representation of a continuum-removed spectrum and annotations demonstrating the anatomy of the parameters calculated for quantitative spectral analyses and plotted in Figures 7 and 8. The dashed line along the top of the 'Nontronite Lab Sample' spectrum (light blue) represents the continuum, which, once determined, is then divided out of the lab sample spectrum to produce the 'Continuum Removed' spectrum (dark blue) at the top of the plot. Note the shoulders of each absorption feature reach, or nearly reach, a normalized reflectance value of 1 which provides a standard of comparison from one spectrum to another.

2.2 CTX and HiRISE Data Processing and Analysis

To correlate spectral variations with surface morphology and ensure that the measured CRISM pixels correspond to geological variations rather than instrument noise, we used base maps of mosaicked images from the High Resolution Imaging Science Experiment (HiRISE) and Context Camera (CTX), which are both aboard the MRO. CTX produces visible wavelength images which are roughly 6 m/pixel (Malin et al., 2007). HiRISE produces visible wavelength images which are roughly 0.25 m/pixel (McEwan et al., 2007). Mosaicked sets of CTX images provided the primary base map for the entirety of the study region (e.g., Figure 3A), and are used

as the standard for georeferencing of other data sets, including HiRISE and CRISM. Mosaicked sets of HiRISE images were also used as base maps, but will primarily for the region that includes the primary deposit (e.g., Figure 4D).

In collaboration with Dr. Tim Goudge of UT Austin, stereo-pairs of both CTX and HiRISE observations were used to construct stereo-photometry-derived digital elevation models and corresponding ortho-images covering the study region. DEMs were produced using the NASA Ames Stereo Pipeline (ASP) (Broxton and Edwards, 2008; Moratto et al., 2010; Shean et al., 2016). The ASP was also used to tie CTX and HiRISE point clouds to MOLA point shot data to minimize error associated with regional slope (Beyer at al., 2014). CTX DEMs have a vertical error of ~6 m/pixel and the HiRISE DEMs have a vertical error of ~0.25 m/pixel (Fassett et al., 2016). A full list of the CTX and HiRISE images used in this study can be found in Table 3.

Table 3: List of CTX and HiRISE Images Used

Observation ID	Observation Type
B21_017911_1559	CTX
B21_017700_1557	CTX
B02_010619_1561	CTX
G02_019111_1548	CTX
B22_018333_1548	CTX
B02_010263_1557	CTX
B02_010263_1557	CTX
B22_018122_1555	CTX
B02_010408_1548	CTX
B03_010830_1560	CTX
P21_009274_1558	CTX
B10_013599_1559	CTX
B10_013454_1559	CTX
D04_028803_1558	CTX
D04_028592_1558	CTX
G02_019111_1548	CTX
G01_018689_1548	CTX
G04_019757_1542	CTX
G05_020034_1543	CTX
ESP_047119_1560	HiRISE
PSP_001336_1560	HiRISE
ESP_019757_1560	HiRISE
ESP_028803_1560	HiRISE
ESP_018412_1560	HiRISE

2.3 Modeling Crater Ejecta Thickness, Calculating Clay Volumetric Distribution, and Measuring Channel Incision Depth

We made use of the Barnhart and Nimmo (2011) impact model that estimates radial distribution of ejecta blanket thickness and the volumetric proportion of clays within an ejecta blanket. The model employs a modified Maxwell-Z model, which is an empirically derived approach for describing subsurface flow fields for planetary scale impacts based on observations of parcels of material ejected from nuclear detonations (Maxwell, 1977). Barnhart and Nimmo (2011) track ejecta material from pre-impact sub-surface origins to post-impact destinations, providing an estimated volume ratio of clays for craters in Noachian aged surfaces (e.g., Figure

6). This model takes a crater size (radius in km), clay layer thickness (m), and clay layer burial depth (m) as inputs. We used a clay layer thickness of 30 and 100 m on the basis of the results from Le Deit et al. (2012), who found a ~30 m thick regional layer of phyllosilicate clays in the vicinity of our study area. Le Deit et al. (2012) observed this layer at a variety of elevations and locations. In some locations it was found to be exposed at or near the surface, and at other locations it was found to be buried by tens of meters of overlying strata. For this reason, we have chosen to test burial depths of 0 m, 30 m, and 100 m. Crater radii were determined by measuring both the Holden and Eberswalde craters in Google Earth, and they were found to be 75 km and 35 km respectively. The Barnhart and Nimmo (2011) model assumes a buried clay-rich layer to be 100% clay by volume, however the highest estimates for clay abundances in clay-rich environments is ~50% in Mawrth Vallis (Poulet et al., 2008). The Mawrth Vallis region is a reasonable analog for this study on the basis of a buried clay-rich layer, likely formed via aqueous alteration (Loizeau et al., 2007). To account for this limitation, we assume a clay abundance of ~50% for our buried clay-rich layers in the reported model runs. As such, the clay fraction results of this model reported here should be seen as an upper bound based on the current understanding of martian clay-rich sedimentary deposits. The high temperatures associated with planetary impact events of this scale also plays a role in establishing these results as upper bounds. Shock induced heating has the potential to denature the phyllosilicates in the buried clay-rich layer, as Barnhart and Nimmo (2011) point out. Their analyses of these effects on the volume percentage of clays in the ejecta indicates that for craters with diameters less than 100 km (e.g., Eberswalde crater), the shock induced heating is likely to have a minimal impact. For craters with diameters greater than 100 km, some portion of the excavated clays may be denatured by the high temperatures, however, the region of the impacted rock that sees the highest temperatures, particularly those sufficient to denature buried clays, is focused within the central portion of the impact. As Figure 6 shows, most of the excavated material from this area is not emplaced in the ejecta layers (the dotted lines going out of the top of the plot are ‘lost’). For this reason, while

some percentage (~5% according to Barnhart and Nimmo, 2011; their Figure 7) of Holden's emplaced clays would be denatured, this modeled clay fraction within the ejecta is a reasonable upper bound.

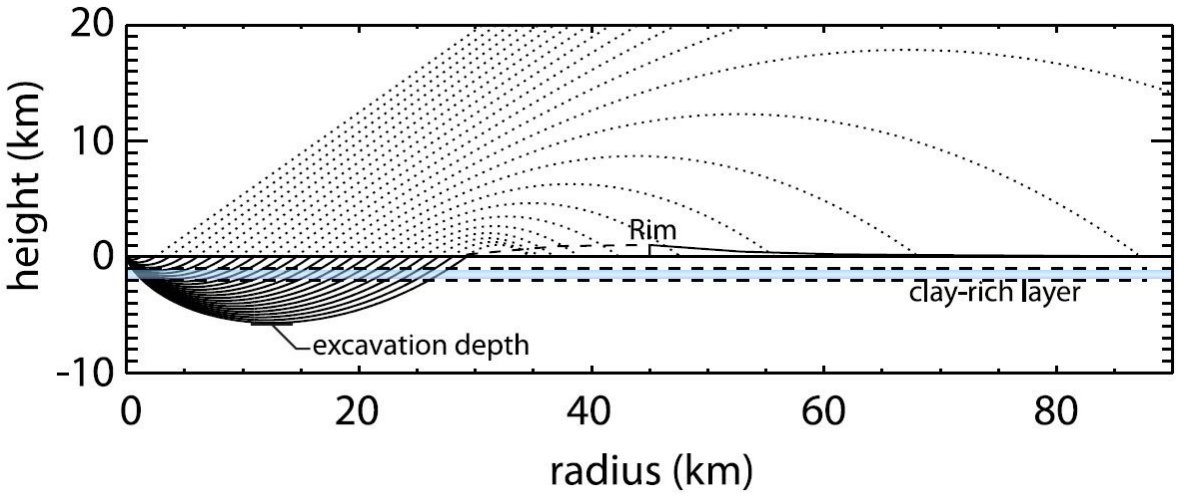

Figure 6: Graphical representation of the modified Maxwell-Z model used in this study for a ~90 km diameter crater (modified from Barnhart and Nimmo, 2011; their Figure 1). The origin represents the center of the crater, and the dotted lines represent the trajectories (stream tubes) of ejected material. The crater rim is labeled, and the blue layer between parallel dashed lines beneath the 0 km height indicates the bounds of a buried clay-rich layer. Stream tubes exiting through the top of the graphic represent material that does not contribute to the emplacement of the impact ejecta deposit.

We used the distribution of ejecta blanket thickness results of the Barnhart and Nimmo (2011) model to test whether the erosional channels of the Eberswalde watershed incise deeply enough to erode through the entirety of the craters' ejecta and into the putative Noachian bedrock below. We calculated an estimate of incision depth of a particular place along a valley traverse within the Eberswalde watershed using CTX DEMs to find an average of the peak elevations of the two valley walls, and then subtracting that average from the elevation at the valley bottom. Valley wall peak elevations are defined by a roll over in the topography or the transition from steeply-sloping valley cliffs to the shallow sloping background topography. Elevation values are calculated by drawing a topographic profile perpendicular to the long axis of the valley in GIS software, ESRI's ArcMap. We compare this incision depth to the thickness of the ejecta stratigraphy results from applying the Barnhart and Nimmo (2011) model to Holden and

Eberswalde craters. If the incision depth exceeds the thickness of the cumulative thickness of both the Eberswalde and the Holden crater ejecta blankets at a particular measuring point then we consider the valley to have eroded into Noachian bedrock. For each prominent valley in the watershed, we make numerous measurements along the length of each valley. Measured valleys are labeled with letters in Figure 3A. The first measurement for each valley was made from the highest elevation regions, and the following measurements were made in the down slope direction at approximately regular intervals of 2 km. We paid particular attention to the valley reaches that show the greatest relief in the DEM. We also closely examined the walls and bottom of each incised valley in a search for any visual evidence of stratigraphic contacts; no such contacts were discovered. However, evidence of the valleys incising through impact breccia has been reported by Mangold et al. (2012) (e.g., their Figure 4) and Irwin et al. (2015) (e.g., their figure 5). Both previous studies note large blocks of light-toned material within the valley walls of the Eberswalde crater fluvial system.

3. Results

3.1 Mineralogy of the Northwest Noachis Terra

The ratioed spectra extracted from the NT region and Holden crater (Figure 2C) have minima within the ~2.29-2.33 μm region commonly associated with the metal-OH absorption band in phyllosilicate clays, and minima within the ~1.91-1.93 μm region associated with the water overtone feature in hydrated minerals (Clark et al., 1990). Some spectra (e.g., purple spectra labeled ‘bece’ from CRISM observation frt0000bece) show signs of additional minima at ~1.40 μm, and ~2.40 μm. The hydrated hydrothermal alteration mineral, vermiculite, has a water overtone features at ~1.40 μm and ~1.92 μm along with a metal-OH absorption feature at ~2.32-2.33, however, none of the CRISM spectra show an indication of the ~2.25 μm present in the lab spectra of vermiculite (magenta spectrum in Figure 2D). Furthermore, based on terrestrial observations, our understanding of the conditions and protoliths typical for the formation of vermiculite may be uncommon on Mars (e.g., Krzensinska et al., 2019; Wilson 2004), although

some authors have noted it as a possibility from CRISM data (e.g., Dehouck et al., 2010; Michalski and Niles, 2010). Chlorite also has the water overtone at ~1.40 μm and a metal-OH absorption feature at ~2.32-2.33, but chlorite has a water overtone feature with minima centered at ~2.00 μm rather than ~1.90 (e.g., blue spectrum in Figure 2D), which is inconsistent with the CRISM spectra. Chlorite also has a relative maximum in the ~2.40 μm region, which is inconsistent with several of CRISM spectra. Nontronite and saponite have metal-OH absorption features centered at ~2.29 and ~2.32 μm, and water overtone features centered at ~1.40 μm and ~1.90-1.92 μm, along with local minima centered at ~2.40 μm (e.g., lab spectra in Figure 2D). Given the consistency in the metal-OH, water overtone bands, and the additional minima at ~2.40 for some spectra, nontronite and saponite are most consistent with the CRISM observations in the NT region. However, given the slight shift toward longer wavelengths in both the metal-OH bands and the water overtone bands (e.g., Figure 7) and the broader FWHM values for some of these spectra (Figure 8), it remains possible that the observed spectra represent a mixed layer of the Fe/Mg clays, saponite and nontronite, and vermiculite, chlorite, and/or some other mineral phase not yet considered. These results are broadly consistent with those of Buczkowski et al. (2010a), Buczkowski et al. (2013), and Le Diet et al. (2012).

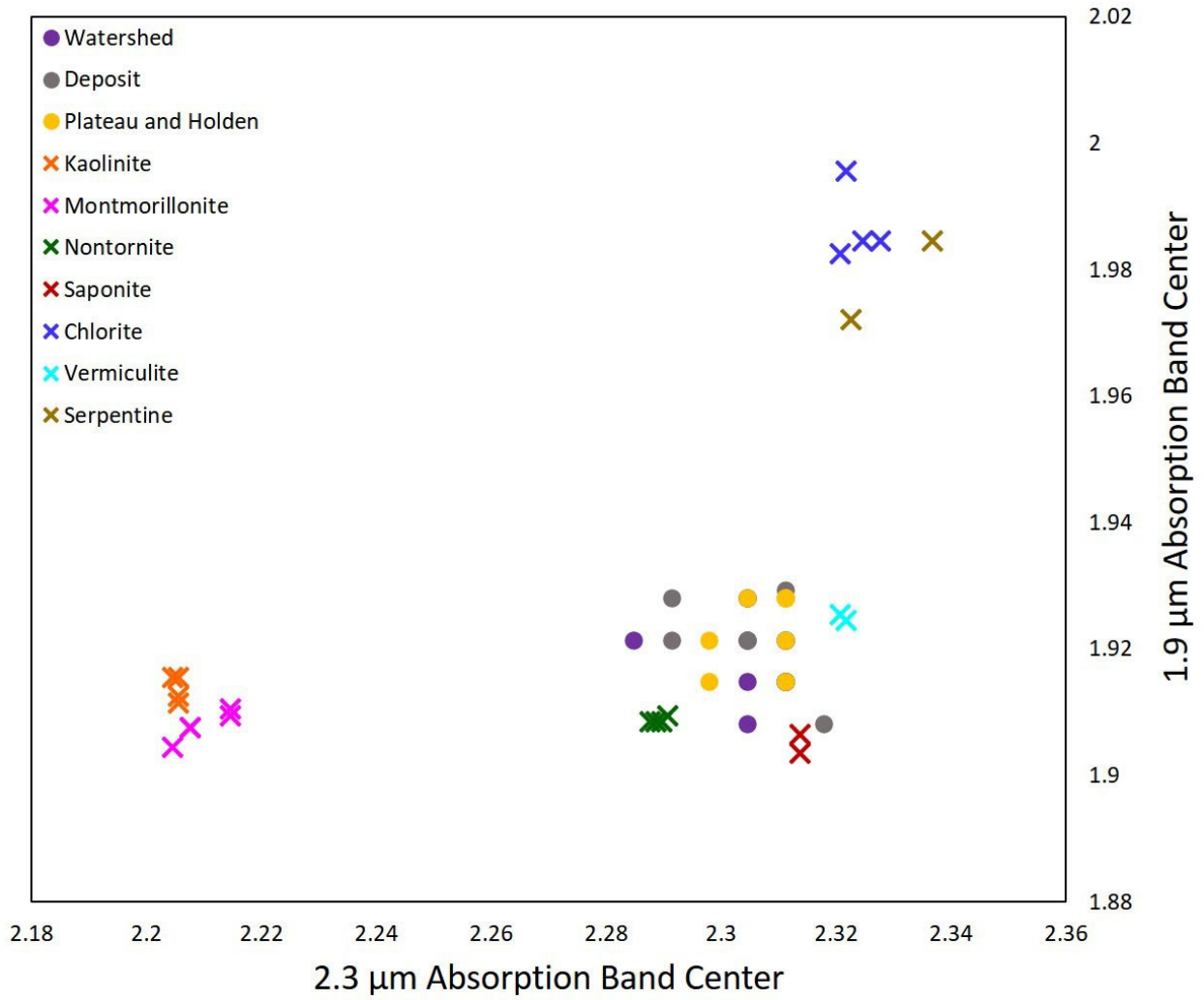

Figure 7: Comparison of measured absorption parameters (method of measurement described in section 2.1 and Figure 5) from extracted CRISM spectra (marked with dots) to a suite of lab sample mineral spectra (marked with X's). Parameters shown here are the precise minima position of the ~2.2 - 2.3 µm absorption features and the precise minima position of the ~1.9 µm absorption features. Note the correlation of the CRISM spectra and the Nontronite, Saponite, and Vermiculite lab samples. CRISM instrument error is ~1% (Murchie et al., 2007).

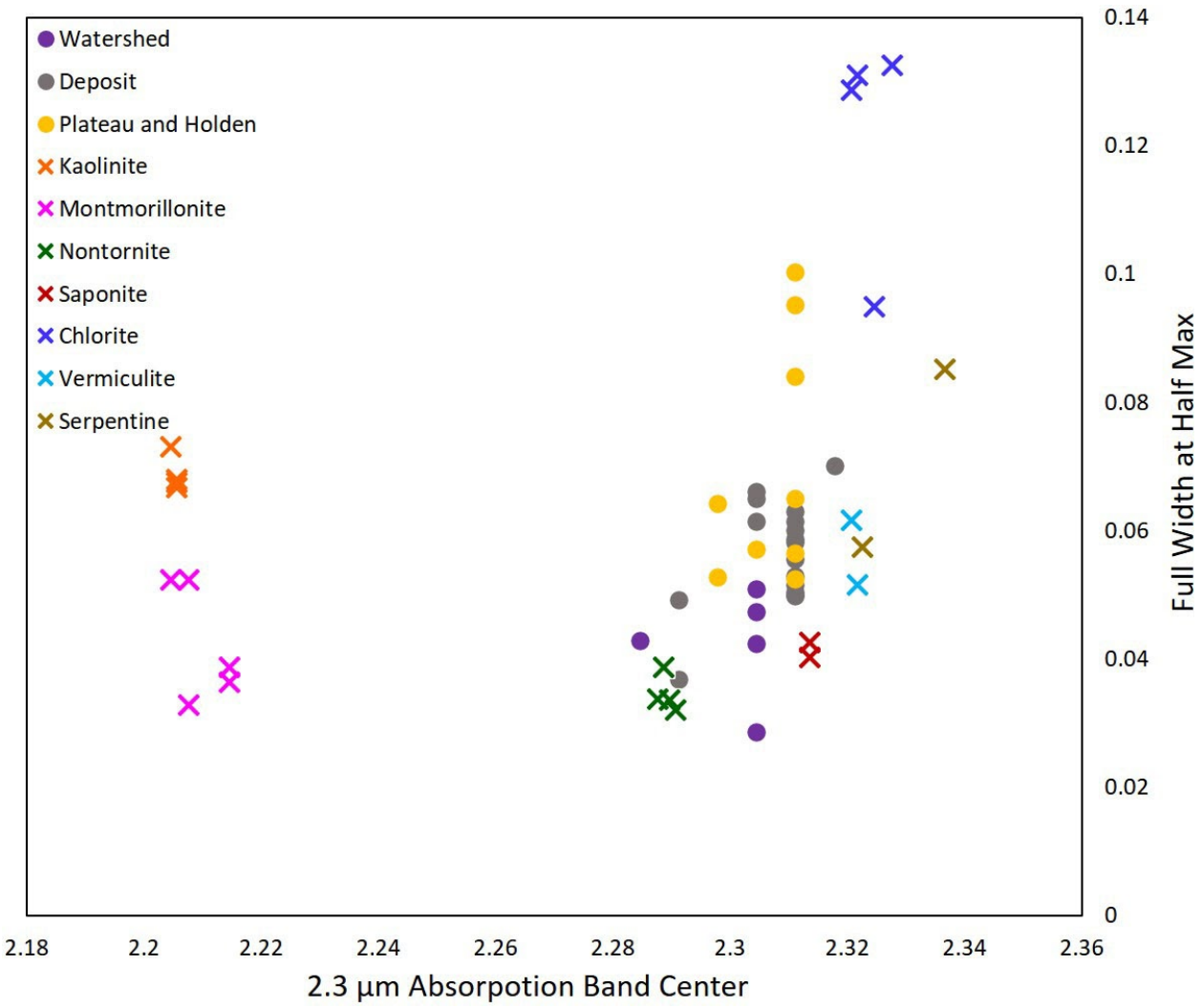

Figure 8: Comparison of measured absorption parameters (method of measurement described in section 2.1 and Figure 5) from extracted CRISM spectra (marked with dots) to a suite of lab sample mineral spectra (marked with X's). Parameters shown here are the precise minima position of the ~2.2 - 2.3 µm absorption features and the full-width at half-max value (FWHM) for the same feature. Samples with a smaller FWHM value are likely composed of a purer phase of a given mineral than those with a larger FWHM value. CRISM instrument error is ~1% (Murchie et al., 2007).

3.2 Mineralogy of the Eberswalde Crater Watershed

We found two FRT CRISM observations to be useful for assessing the mineralogy within the Eberswalde crater watershed, (1) frt0000b2d4 which covers fluvial deposits within a small basin that lies in the middle of the watershed outside of both Eberswalde and Holden craters (Figure 3A, B, and C), and (2) frt0000ccf6 which covers a region in the southeast side of the

watershed (Figure 3A, D, and E). The summary parameter PHY (Viviano-Beck et al., 2014) was useful for identifying regions that have spectral evidence of phyllosilicate clays within the bounds of these two observations (Figure 3C and D). Observation frt0000b2d4 shows a strong spatial correlation between the light-toned exposed layers of the fluvial deposits and red, blue, and magenta CRISM parameter map pixels which correspond to absorption features in the ~2.3 μm region, absorption features in the ~1.9 μm region, and a combination of these two features respectively. ROIs were drawn around exposures where these parameters were spatially extensive, had a demonstrable correlation with a geologic feature in the CTX image, and could be easily discerned from the columnar noise of the CRISM observation. The locations of these ROIs can be seen in Figure 3B and C as color coded and labeled ellipses. Within the bounds of observation frt0000ccf6, there were two regions with concentrations of red and or magenta pixels in the PHY parameter map which are correlated with a crater rim (cyan ellipse labeled B in Figure 3D) and a the topographically high feature (magenta ellipse labeled A in Figure 3D and E) with surface morphology and texture consistent with what previous studies identified as Holden crater megabreccia (e.g., Mangold et al., 2012 and Rice et al., 2013) (Figure 3E). The resulting ratioed spectra from the Eberswalde watershed (Figure 9A) show minima within the ~2.29-2.33 μm region associated with the metal-OH absorption band in phyllosilicate clays, and minima within the ~1.91-1.94 μm region associated with the water overtone feature in hydrated minerals (Clark et al., 1990). Some spectra also show subtle signs of absorption features at the ~2.40 μm wavelength (e.g., blue spectra labeled D in Figure 9A). As with the spectra from NT, these results, along with the measured FWHM values, are most consistent with some combination of Fe/Mg smetites, nontronite and saponite, with the possible presence of chlorite and vermiculite (Figures 7 and 8). Several spectra also have relative minima in the ~2.12 μm region. Absorption features centered around ~2.12 μm are associated with serpentine (e.g., Figure 2D). Serpentine is not a commonly identified mineral in the martian scientific literature, in part due to the weakness of the often diagnostic ~2.12 μm absorption feature (e.g., Ehlmann et al., 2010). However, Ehlmann et al.

(2010) do report identifying serpentine deposits in the ejecta of a small number of craters in the southern highlands of Mars. Ehlmann et al. (2010) also report that serpentine deposits on Mars are frequently found associated with Fe/Mg smectite clays and chlorite deposits, consistent with our observations here.

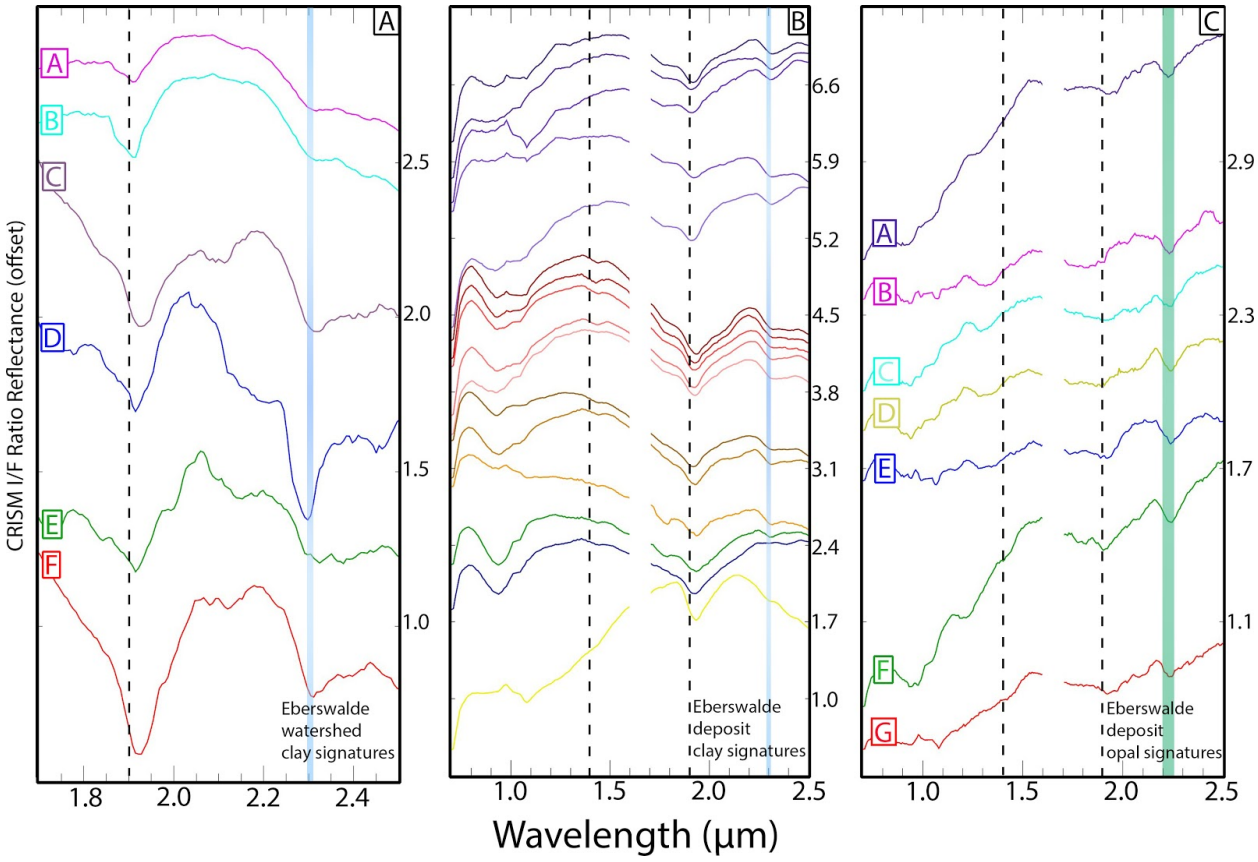

Figure 9: Ratioed and I/F corrected spectra extracted from CRISM observations of the Eberswalde crater fluvial system. Spectra are smoothed using a moving box-car average with the two closest data points on either side of a particular bandpass. Colored-coded letters adjacent to spectra in (A) and (C) correspond to ROI indicators from Figure 4. Spectra in all plots are offset for clarity, and reflectance values labeled on the right side of each plot are relative. The dashed vertical lines indicate the approximate location of the ~1.4 μm and ~1.9 μm water overtone absorption features. The blue and green vertically oriented rectangles correspond to the ~2.29-2.32 μm metal-OH absorption feature in Fe/Mg smectite clays and the broad ~2.21-2.25 μm Si-OH absorption feature in opaline silica respectively. CRISM instrument error is ~1% (Murchie et al., 2007). (A) Spectra extracted from the Eberswalde crater watershed region (Figure 3). (B) Spectra extracted from the Eberswalde putative delta deposit (Figure 4) that are most consistent with Fe/Mg smectite clays (Figure 2D). Spectra are ordered in accordance to their stratigraphic position using elevation as a proxy (e.g., Figure 4D). (C) Spectra extracted from the Eberswalde putative delta deposit (Figure 4) that are most consistent with opaline silica (Figure 2D).

3.3 Mineralogy of the Eberswalde Crater Deposit

Half resolution (~36 m^2/pixel) CRISM MTRDR observation hrs00003207 covers the majority of the putative deltaic deposit within Eberswalde crater (Figure 4A, B, and C) including the erosional front where the exposed layers of deltaic deposit can be investigated individually (Figure 4D and E). Summary parameter maps HYS (Figure 4B) and PHY (Figure 4C and E, Viviano-Beck et al., 2014) generated from this CRISM observation were useful in correlating geologic features with spectral parameters consistent with opaline silica or phyllosilicate clays respectively.

As stated previously, Poulet et al. (2014) noted the possible presence of opaline silica material in the vicinity of this deposit, and we confirm their results here (Figure 4B and 8C). We note that in the HYS parameter map (Figure 4B) there is an absence of green (BD2250), red (MIN2250), or yellow (BD2250 + MIN2250) pixels (which correspond to Si-OH absorption features in the ~2.21-2.25 μm region) on the erosional front of the deposit (right side of the image), and instead that region is dominated by blue (BD1900r2) pixels (which correspond to the water overtone absorption feature centered about ~1.91 μm). This indicates that, while the erosional front of the deposit shows a strong spectral indication of hydrated mineralogy, there is limited evidence for the presence of hydrated opaline silica in this region. The top surface of the deposit is pervasively speckled with green (BD2250), red (MIN2250), or yellow (BD2250 + MIN2250) pixels in the HYS parameter map (Figure 4B), but there is not a discernible correlation between geologic features and the spectral parameters. The main geologic feature in the region, topographically-inverted channel deposits, are as consistently covered in spectral indications of opaline silica, as are the spaces between them. Nevertheless, there are concentrated regions of these opaline silica indicators that are discernible from CRISM columnar noise, and several of these were sampled with ROIs (colored and labeled ellipses in Figure 4B), and their ratioed spectra are reported in Figure 9C. Each of these spectra have a broad absorption in the ~2.21-2.26 μm region consistent with laboratory spectra of opaline silica (Figure 2D), and show weak

signals of ~1.90 μm hydration bands. Many of the spectra also present with subtle indications of the ~1.40 hydration band.

In the PHY parameter map (Figure 4C and E), there is an visibly evident correlation between the deltaic stratigraphy exposed at the erosional front of the deposit and red (D2300), blue (BD1900r2) and magenta (D2300 + BD1900r2) pixels which correspond to Fe/Mg-OH absorption features in phyllosilicates, the water overtone absorption feature centered about ~1.91 μm, and a combination of these two parameters respectively. We also note a dearth of green pixels (BD2200) in this parameter map, except in locations that also correspond to the presence of hydrated silica from the HYS parameter. The absence of a signal from the BD2200 parameter in this region is consistent with a lack of spectral evidence of alumino silicates, such as montmorillonite or kaolinite (e.g., Figure 2D).

We sample at various levels within the vertical stratigraphic succession, with ROIs drawn within the highest elevation stratal surfaces (youngest deposits) shown in Figure 4D with hues of purple and pink. We then proceed down the stratigraphy with a group of red ROIs drawn along a putative stratal plane testing variability in the lateral extent of that layer. After the red layer comes a group of ROIs with golden hues, which are followed by a single green ROI, and then a blue ROI drawn on the oldest layers of the deltaic deposit. The yellow ROI is drawn over what has been identified as a piece of Holden crater megabreccia (Rice et al., 2013a). The resulting ratioed spectra from these ROIs are reported in Figure 9B and the vertical stratigraphic succession is preserved in that plot with the youngest layers at the top of the plot (ROIs with purple and pink hues) and the oldest layers at the bottom (blue is the oldest deposit layer and yellow is older than the deposit itself being Holden megabreccia). The ratioed spectra extracted from the erosional front of the Eberswalde crater deposit have minima within the ~2.29-2.33 μm region commonly associated with the metal-OH absorption band in phyllosilicate clays, and minima within the ~1.91-1.93 μm region associated with the water overtone feature in hydrated minerals (Clark et al., 1990). Many of these spectra also show signs of additional minima at ~1.40 μm, and ~2.40 μm.

As with the geographic regions analyzed above, these spectral characteristics are most consistent with a mixture of Fe and Mg smectite clays, nontronite and saponite. Again, these spectra have minima that are shifted toward slightly longer wavelengths than what would be expected for a mixture of pure nontronite and saponite (Figure 7) and their measured FWHM values are slightly broader than the pure phases represented by the lab samples of nontronite and sapointe (Figure 8), so it remains plausible that these deposits are composed of a mixture of these clays and other aqueous alteration minerals such as chlorite, vermiculite, or some other mineral species not yet considered (Figure 7). These results are consistent with the findings of Milliken and Bish et al. (2010). We do note that all of the spectra from the erosional front also show signs of additional absorption features centered around ~0.90 μm, an absorption feature found in lab spectra of nontronite and chlorite (Figure 2D), further confirming the likelihood of the presence of these minerals. We also note some absorption features around the ~1.1 μm region in several of the spectra from this region (e.g., yellow spectra at the bottom and purple spectra 3rd from the top in Figure 9B). These features may be associated with the presence of olivine which has an absorption band at this location, although the olivine feature in this region is a combination of bands between ~0.84 μm and ~1.25 μm. The consistent presence of this feature in all spectra from this image (Figure 9B and C) to varying degrees indicates this may be an dataset-wide aberration. We observe limited to no evidence for any systematic change within the vertical succession of the delta stratigraphy, or along any given stratal surface.

Full resolution (~18 m^2/pixel) CRISM MTRDR observation frt00009c06 also covers this region (Figure 4A and F) but was not processed for analysis as an MTRDR by JHU-APL until recently, therefore no spectra have been extracted from that dataset at the time of this writing, and the spectra reported here are exclusively from hrs00003207. However, it was possible to confirm the results of the PHY parameter map from hrs00003207 using the same parameter generated from frt00009c06 (Figure 4F). Given the evident similarities between Figure 4C, E and F, it stands to reason that spectra extracted from frt00009c06 would be broadly consistent with

those which we have already extracted from hrs00003207. Further analyses of frt00009c06 will be required to fully characterize this deposit, and to analyze any differences between differently aged depositional lobes (Pondrelli et al., 2011).

3.3 Impact Modeling Results and Incision Depth Analyses

The modeled clay fraction by volume results from the Barnhart and Nimmo (2011) model for Eberswalde and Holden craters are reported in Figures 10 and 11, respectively. We identify the clay-rich layer thickness of 30 m as most realistic, as that is roughly consistent with the measured thickness from Le Diet et al. (2012). Also per the results of Le Diet et al. (2012), we contend that the clay-rich layer is most likely either at or near to the surface (i.e., model runs with depth = 0 m) or buried quite shallowly (i.e., model runs with depth = 30 m). We note the low concentrations in all model runs, particularly for those we suggest are most realistic. We also note the consistent magnitude of the clay fractions in the regions most impacted by valley incision and fluvial transport. The regions of Figures 10 and 11 that are right of the black vertical line indicate where, volumetrically, the majority of the sediment deposited in the delta would have been sourced from this region. These results indicate that, while the clay abundance that resulted from ejecta emplacement may be low as a fraction of the overall ejecta volume, the majority of the spatial extent of the ejecta would be composed of a similar abundance of clay minerals.

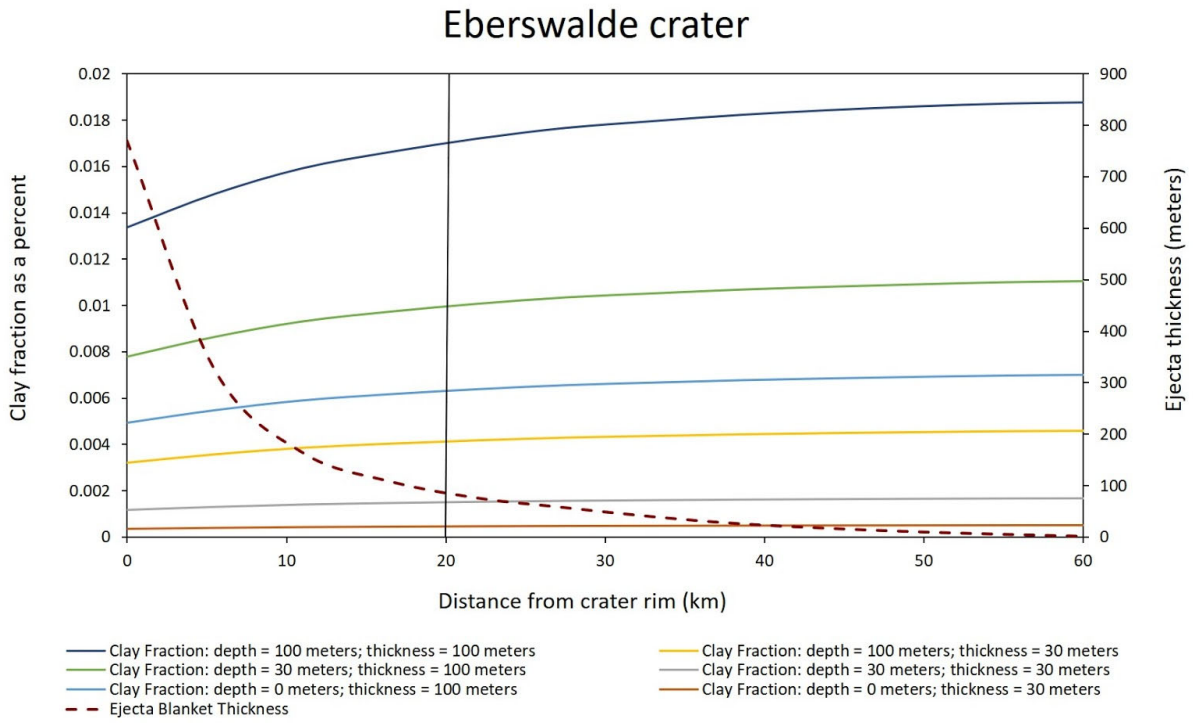

Figure 10: Results of the Barnhart and Nimmo, 2011 model for Eberswalde crater showing the volumetric fraction of clay in the ejecta as a function of distance from the crater rim for various model runs (solid curves), and the thickness of the Eberswalde ejecta layer (dashed curve). To the right of the black vertical line indicates the range of distances where most visibly identifiable valleys incise into the ejecta layers, as seen in Figure 3A (i.e., volumetrically, the majority of the sediment deposited in the delta would have been sourced from this region). We consider model runs with a thickness of 30 m and a burial depth of 0 m or 30 m to be most representative of real possibilities based on observations of nearby clay-rich layers by Le Diet et al., (2012).

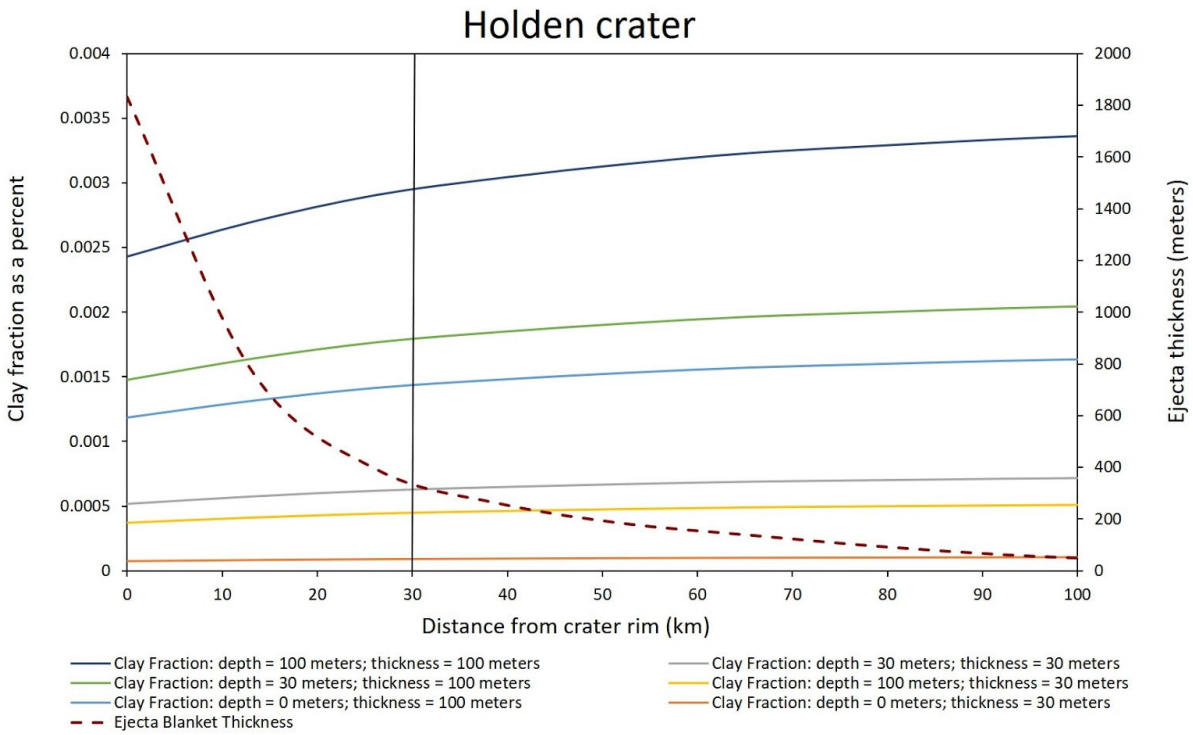

Figure 11: Results of the Barnhart and Nimmo, (2011) model for Holden crater showing the volumetric fraction of clay in the ejecta as a function of distance from the crater rim for various model runs (solid curves), and the thickness of the Holden ejecta layer (dashed curve). To the right of the black vertical line indicates the range of distances where most visibly identifiable valleys incise into the ejecta layers, as seen in Figure 3A (i.e., volumetrically, the majority of the sediment deposited in the delta would have been sourced from this region). We consider model runs with a thickness of 30 m and a burial depth of 0 m or 30 m to be most representative of real possibilities based on observations of nearby clay-rich layers by Le Diet et al. (2012).

The results of our incision depth measurements are reported in Table 4 and Figure 12. These results indicate that the cumulative ejecta thickness exceeds fluvial valley incision depth in all measurable areas of the watershed. That is, there are no regions of the watershed where the erosional valleys incise deeply enough to erode all the way through the ejecta blankets of the Eberswalde and Holden impacts. Our results indicate that the ejecta is substantially thicker than any measurable valley incision within the watershed. The closest any valley came to incising through the modeled ejecta thickness was with location H-2, which incised within 33 m of the putative noachian bedrock/ejecta blanket contact based on our modeling results (Table 4).

Table 4: Results from incision depth calculations. Uncertainty associated with incision depth measurements derived from the vertical uncertainty of the CTX stereo-derived DEMs the measurements were calculated from (i.e., +/- 12 m). Measurements are labeled according to the valley they were taken from (Figure 3A), and with the lowest number, or first measurement along a valley, being taken at the furthest upstream portion of the valley. Measurements are spaced approximately 2 km apart, with particular emphasis on regions with the most apparent incision based on visual inspection of the DEMs.

Measurement	Incision Depth (m)	Eberswalde Ejecta Thickness (m)	Holden Ejecta Thickness (m)	Cumulative Ejecta Thickness (m)	Sufficient Incision?
A-1	169	152	470	622	No
A-2	161	163	442	605	No
A-3	148	188	4066	594	No
A-4	153	218	373	591	No
A-5	152	220	329	549	No
A-6	127	175	307	482	No
B-1	61	86	390	476	No
B-2	38	94	351	445	No
B-3	49	91	327	418	No
B-4	47	95	283	378	No
C-1	78	20	358	378	No
C-2	84	21	336	357	No
C-3	83	22	321	343	No
C-4	113	24	295	319	No
C-5	66	24	267	291	No
D-1	42	9	259	268	No
D-2	63	10	248	258	No
D-3	36	11	241	252	No
D-4	33	15	233	248	No
D-5	22	16	227	243	No
E-1	42	4	210	214	No
E-2	39	5	207	212	No
E-3	83	9	201	210	No
E-4	62	10	198	208	No

E-5	31	14	178	192	No
F-1	29	4	147	151	No
F-2	52	5	146	151	No
F-3	49	6	152	158	No
F-4	26	11	163	174	No
G-1	31	9	64	73	No
G-2	36	13	73	86	No
G-3	30	15	84	99	No
H-1	25	15	51	66	No
H-2	31	17	47	64	No
H-3	38	24	49	73	No
H-4	31	26	53	79	No

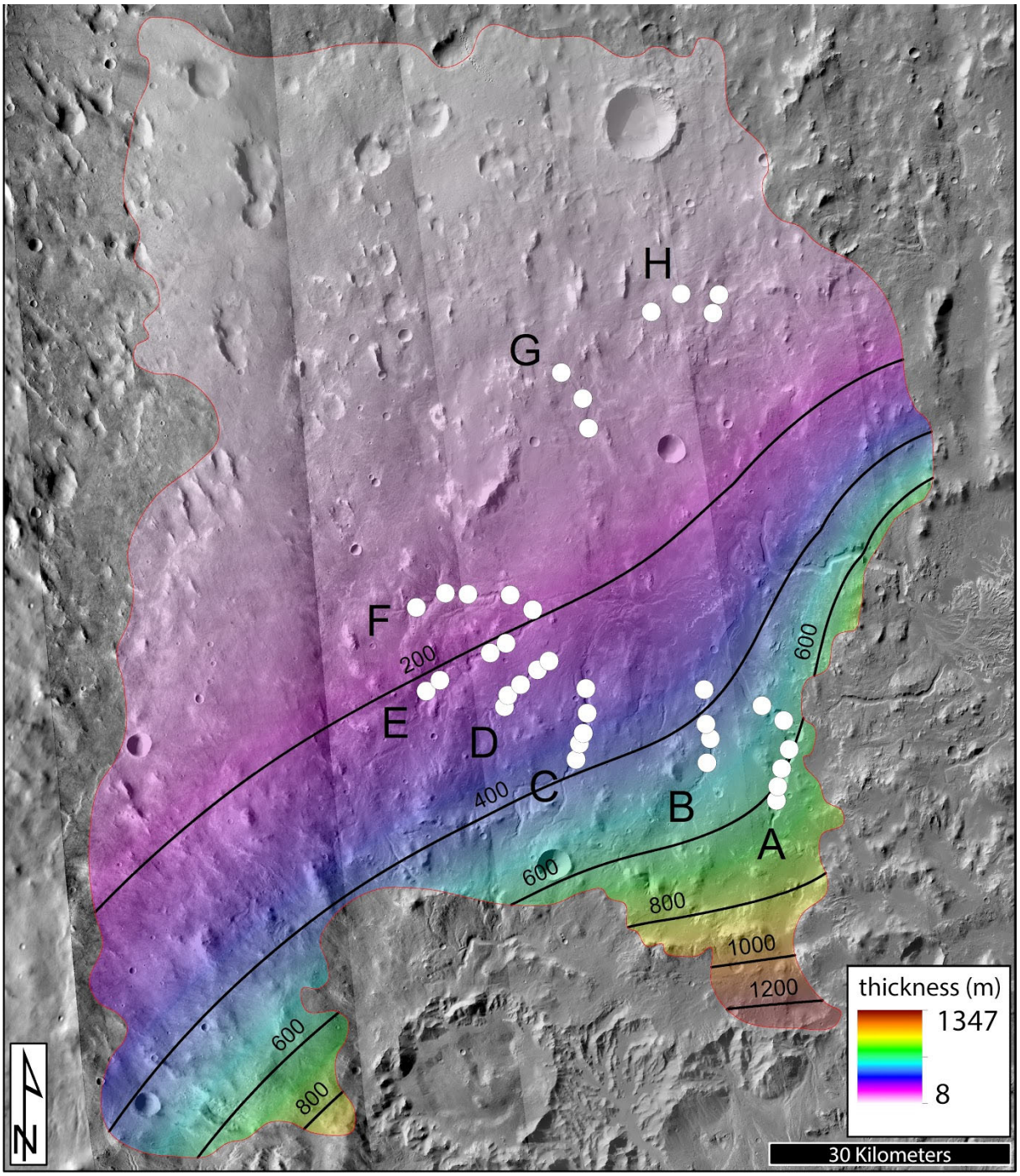

Figure 12: Distribution of modeled cumulative ejecta thickness from both the Eberswalde and the Holden impact events within the bounds of the watershed (Mangold et al., 2012, thin red line) shown with color scale and contour lines (contour interval is 200 m). Image is a mosaic of day-time THEMIS and CTX images B06_011898_1558, J02_045550_1560, B21_017911_1559, B21_017700_1557, B02_010619_1561, G02_019111_1548, B22_018333_1548, and B02_010263_1557. Incision depth locations indicated with white circles, and labeled with capital letters at the head of each valley and increasing in number as you move down the length of the valley in the downstream direction (e.g., measurement A-1 is the furthest upstream along valley A). Measurements were made down the length of the valley and spaced ~2 km apart with a

focus on regions which showed the greatest relief in CTX derived DEMs. Results of the measurements are reported in Table 4. None of the results indicated enough erosion to have incised all the way through the layers of ejecta to reach the pre-impact clay-bearing basement rocks.

4. Discussion

The comparison of the CRISM spectra shows that measurements from all geographic regions that were consistent with Fe/Mg smectite clays are closely grouped when plotted in spectral parameter space (Figure 9). The spectral and mineralogic consistency between the fluvially linked Eberswalde watershed and the Eberswalde crater deposit points to a detrital source for the clays found within the delta deposit. This is a strong indication that these clays formed prior to fluvial transport. If they had formed after transport, we may not expect to find them within the watershed region, and instead only within the crater and the fluvial stratigraphy. Furthermore, if they had formed within the crater, we should expect to find spectral indications of clays at other locations within the crater, which we have not. If they formed during fluvial transport, we may expect to find some variability in the spectral signatures within the vertical succession of layers within the deposit, such as a transition from unaltered detritus to progressively more altered material, but we do not (e.g., Figure 9B). Formation during transport is also inconsistent with results from studies of the Amazon River basin on Earth (Gibbs, 1967), which indicate that the smectite clay forming processes do not take place during active fluvial transport, and instead active chemical processes during transport are limited to ion exchanges in already formed clay minerals (Meunier, 2005). The lack of spectral variability within the layers of the deposit also indicates that there were no dramatic changes in the source regions during the construction of the putative delta deposit.

While there is spectral consistency between the Eberswalde fluvial system (i.e., both the watershed and the deposit) and the “Plateau Phyllosilicates” deposits observed in the NT region (e.g., Figure 2C; Buczkowski et al., 2010a; Buczkowski et al., 2010b; Buczkowski et al., 2013; Buczkowski et al., 2014, Le Deit et al., 2012), our analysis of the incision depth of the erosional

valleys within the Eberswalde watershed indicates that there may not be enough valley incision to erode through the entirety of the layers of ejecta from the Eberswalde and Holden impacts, layers which overlie the ancient Noachian bedrock. Our initial hypothesis was that evidence of fluvial incision into the Noachian-aged subsurface beneath the ejecta layers, where the “Plateau Phyllosilicates” likely reside, would be required in order to verify the possibility that the “Plateau Phyllosilicates” may be the same as those found within the Eberswalde watershed and crater deposit. However, the incision depth measurements (Table 4) are made on modern geomorphic surfaces, which may have minimal resemblance to the ancient surface present when the rivers were actively eroding into the martian surface in the late Hesperian (Figure 1). In the time since the cessation of fluvial activity when these valleys were possibly at their deepest (early to mid Amazonian; Figure 1), erosion may have reduced the elevation of valley walls, and valley bottoms may have been filled through depositional processes. These circumstances would skew these measurements toward being minimum approximations. Still, other researchers have shown that aeolian erosion may accentuate valley morphology (e.g., Perkins et al., 2015), which may skew these measurements towards being maximum approximations. Furthermore, many hundreds of millions, or even a billion+ years, elapsed between the emplacement of the ejecta (late Noachian to early Hesperian for Eberswalde impact and Hesperian for Holden; Figure 1) and the period before the onset of fluvial activity (Hesperian; Figure 1). During this time, it is possible that aeolian activity produced sufficient deflation of the surface to erode most of, or the entirety of, the Eberswalde ejecta blanket. Although, this is unlikely to be the case for the Holden ejecta blanket, as remnants of this ejecta layer have been identified by visual inspection (e.g., Mangold et al., 2012). Nevertheless, despite some remnants of the Holden ejecta remaining visually identifiable, it is possible that a significant portion of the initial thickness of this layer may have been removed by aeolian erosion. It is also possible that during the period of time prior to fluvial incision but after the impact events, there was significant aeolian deposition which added to the overall thickness of layers above the Noachian phyllosilicate bearing bedrock. Evidently, environmental and

temporal factors introduce significant and unknown amounts of uncertainty in both directions for these measurements, and so, we suggest they should be seen simply as a starting point for a problem that remains largely underconstrained and underdetermined. For this reason, and despite the results of our measurements, we still consider it a possibility that the fluvial network in the Eberswalde watershed region may have eroded into intact Noachian aged clay-rich layers beneath the layers of impact ejecta, if not least given the similarity in the mineral assemblage between the geographic regions.

It is also possible that emplacement of clays in the watershed took place through relocation from the subsurface to the ejecta blanket layers following the Eberswalde and Holden impacts. We see evidence of this from the observation of smectite clay signatures from spectra extracted from rocks identified as Holden impact megabreccia (e.g., Figures 3D, 3E, 4D, and 4E). The Barnhart and Nimmo (2011) model results also indicate that the clays in the ejecta blankets represent a small volumetric proportion of the overall material emplaced during the impact event (Figures 10 and 11). However, studies of terrestrial fluvial systems reveal smectite clay mineral grains in fluvial transport are predominantly sufficiently small grain sizes (Gibbs, 1967) to be primarily transported as colloids (i.e., particle sizes ranging from 0.1 - 1.0 μm) (Meunier, 2005). This is significant because the settling velocity of a colloidal particle is impeded by the Brownian motion acting on that particle (Meunier, 2005), which allows them to be transported great distances in suspension even during low flow-velocity conditions. Therefore, the strong spectral signature of the smectite clay minerals in the erosional front of the deposit (which coincides with the most distal region of the preserved fluvial system) may be the result of the long transport distance and resultant concentration of these small-sized smectite grains in the most distal portions of the Eberswalde fluvial system. Also, considering the consistent volumetric proportion of smectite clays within the watershed (Figures 10 and 11) and the watershed's significant lateral extent (watershed outlined in red in Figure 3A from Mangold et al., 2012), the fluvial system had substantial space and time to concentrate clays from the watershed into a significant volumetric

proportion of clays in the distal portions of the deposit, which explains the strong spectral signal observed there (Figure 4C, E and F).

The small grain size of the smectite clays may play a role in why they are observed within the stratigraphy of the small inter-basin deposit shown in Figure 3B (light-toned outcrops in the center of the panel). Pondrelli et al. (2008) noted these deposits, and the small basin where they lie, and suggested this may be an older, now dissected, crater that acted as an intermediate sink. Whether the 'mini basin' was home to a standing body of water is not clear, however. It is quite evident, though, that the clay-bearing layers we observed there were eroded into at a later time (Figure 3B). This erosion indicates changing base level downstream of this 'mini basin'. Such a change in base level could be brought about by a knick point migrating upstream after the breach of the Eberswalde crater wall that started the filling of the crater and the formation of the crater lake. This would mean that the early stages of fluvial activity resulted in water and sediment filling the small inter-watershed basin with water and sediment, until the breaching of Eberswalde crater's western wall. The breaching event then resulted in the 'mini basin' draining of water, and the remobilisation of sediment transported from the 'mini basin' to Eberswalde crater. This small inter-watershed basin also raises questions about the intermittency of the fluvial activity in this region, as it seems plausible that the cross-cutting relationships between the erosive channels and deposits may also point to several stages or periods of fluvial activity. It is possible that these deposits represented a separate and older period of fluvial activity, and that the small basin there was the most distal portion of an older source-to-sink system. As such, the deposits, their observed mineralogy (Figure 9A), and the stratigraphy in this mini basin present new interesting questions and untested hypotheses about the evolution of the Eberswalde fluvial system.

The results indicating the relatively consistent proportion of clays within the ejecta blankets of the Eberswalde and Holden impact also have implications for the other smaller fluvial and alluvial deposits identified within Eberswalde crater (e.g., Goddard 2013; Rice et al., 2013a). If the mineralogy we see so evidently in CRISM observation hrs00003207 (e.g., Figure 4C and E)

is sourced from the ejecta layers within the watershed region, and the watershed has such a consistent composition of smectite clays (Figures 10 and 11), then it stands to reason that the source regions of those other fluvial/alluvial deposits may be of similar composition. And, provided that the transport mechanisms for those deposits were relatively similar (i.e., sediment transport over long periods of time and distances sufficient for grain size fractionation), we may expect to find a similar composition of minerals within those deposits. We did examine the available CRISM data to test this hypothesis (Table 1), but were not able to find any substantive evidence indicating the presence of smectite clays in other deposits within Eberswalde crater. This may be the result of the diminutive nature of the other fluvial/alluvial deposits implying transient or short-lived transport timelines, the small transport distances (e.g., Goddard, 2013), or dust-cover obscuring the spectral signature of the clay mineralogy.

The excavation of buried clay-rich sediment may not be the only source of clays within the watershed, though, as recent work examining the formation of smectites in impactites from the Reis impact crater in Germany points to the possibility that the smectite clays may form as a result of hydrothermal activity following impact crater events. Caudill (2020) find evidence of Al, Fe, and Mg smectites in the ejecta deposits of the Reis crater, however the absence of spectral evidence of Al smectites within the Eberswalde system is not a clear indication of the absence of those minerals. Mosser-Ruck et al. (2003) have also shown, under experimental hydrothermal conditions, that alteration from vermiculite to a mixed composition of saponite and chlorite is possible, and given our results indicating the possibility of a mixed composition of all three of the minerals (e.g., Figure 7), we consider the post-impact hydrothermal alteration of pre-existing clay or mafic material a plausible scenario.

Spectral signatures consistent with opaline silica are observed only on the deposit top, and not within the layers of the putative delta stratigraphy (Figure 4B). This observation indicates that the period of alteration that formed the clays and the period of alteration that formed the opaline silica deposits were separate events, as they are stratigraphically distinct from one

another. The lack of a consistent correlation between the geologic features of the deposit top (e.g., the pervasive topographically-inverted channel deposits) and the spectral signatures of the opaline silica deposits indicates that the formation of these deposits may have happened subsequent to the period of fluvial activity. However, if we assume that the opaline silica is temporally or genetically linked to the fluvial activity and we reconsider our understanding of the dominant grain size of the smectite clays and their concentration in the distal portions of the deposit, the larger grains transported by this fluvial network would have remained further upstream and in the region dominated by inverted channel deposits (Figure 4A). In line with this interpretation, the weakness of the hydration bands from the spectra that are most consistent with opaline silica (Figure 7C) could be due to mineralogic and spectral mixing with darker mafic material, as has been shown by the results of Pommerol and Schmitt, (2008). Unaltered mafic mineral grains have greater densities and typically larger grain size than aqueous alteration products such as smectite clays (e.g., Garzanti et al., 2008; Gibbs 1967). Therefore, they are less readily transported by fluvial processes, and may be expected to remain in the more proximal regions of a deltaic deposit. On Mars, opaline silica has also been observed to be the result of alteration of the predominantly mafic materials of the martian crust (Milliken et al., 2008). Therefore, another possible explanation for the presence of the opaline silica present on top of the Eberswalde crater deposit is via weathering and alteration of mafic detritus transported from the Eberswalde watershed. Although, Rice et al. (2013b) have shown that the volume of H_2O and OH absorbed by the silica gel during formation is another possible explanation for the weakness of the opaline silica hydration bands.

We propose the following sequence of events happened in this region (Figure 14): (1) the “Plateau Phyllosilicates” form in the Noachian, (2) Eberswalde crater forms in the late Noachian or early Hesperian distributing “Plateau Phyllosilicates” by crater ejecta, (3) Holden Crater forms in the middle Hesperian also distributing “Plateau Phyllosilicates” by crater ejecta, and (4) the fluvial network and deposit form in the middle/late Hesperian or the early/middle Amazonian.

These events, when taken together with the evidence of spectral consistency of smectite clay minerals between the regions, the remaining possibility that the fluvial system may have incised into the buried smectite clay layers, and the consideration of the concentration of fine grained smectites in the distal regions of the deposit, point to the possibility that the clays observed in abundance within the Eberswalde crater deposit formed during the Noachian period in the subsurface. Noachian subsurface conditions are what some researchers have pointed to as the most likely to preserve evidence of past life (e.g., Ehlmann et al., 2011, Azua-Bustos et al., 2020). Given that the visibly identifiable fluvial system within the watershed covers a vast geographic region, and the prior extent of that system is significantly larger (e.g., Figure 3A; Mangold et al., 2012), the main putative deltaic deposit may preserve a substantial record of rocks from previously habitable environments concentrated in one rover-accessible area. Furthermore, the presence of detrital smectite clays within the crater lake deposit indicates that, at least during the period of time during deposit formation (minimum duration of 75,000 to 150,000 years during the Hesperian; estimate by Irwin et al., 2015), the lake was close to neutral pH, and may have been a habitable environment during that time (as has been shown for other areas of Mars by Ehlmann et al., 2008 and Goudge et al., 2015b). And, considering the expansion of our understanding of clay formation during and after impact events via hydrothermal alteration (Caudill, 2020), Eberswalde crater provides a unique opportunity to ground truth those results by examining the mineralogy of two crater events that have been concentrated in a single deposit.

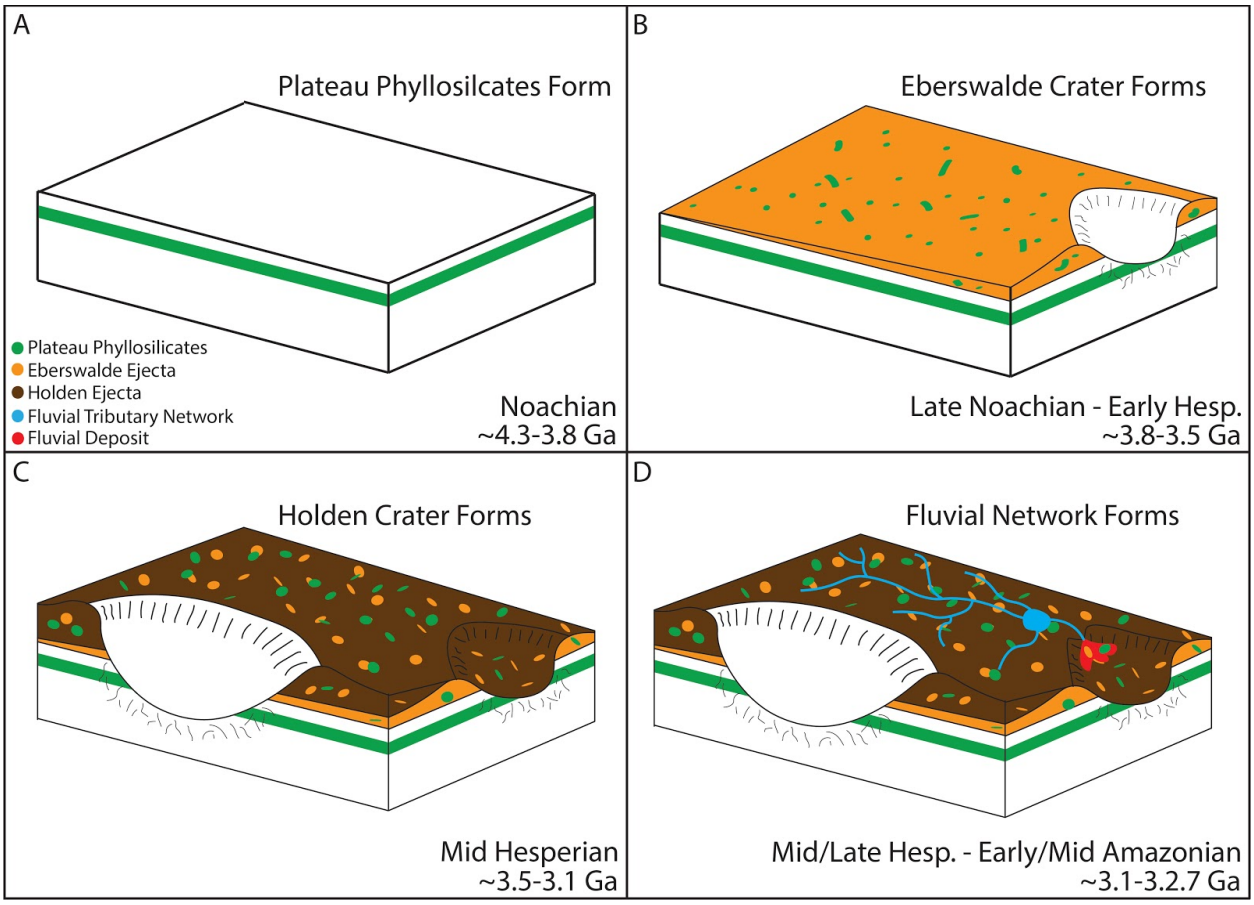

Figure 13: Illustration of the interpreted sequence of events that lead to the concentration of subsurface sourced smectite clays in the main Eberswalde river delta deposit (red polygon in panel D). (A) "Plateau Phyllosilicates" (green layer) form in the subsurface through pedogenic processes (Le Diet et al., 2012). (B) Eberswalde crater forms creating an ejecta blanket (orange layer) that distributes smectite clays over the region. (C) Holden crater forms creating an ejecta blanket (brown layer) that distributes smectite clays over the region. (D) Fluvial network forms (blue lines) and erodes into ejecta blankets and possibly through them, to transport smectite clays to the delta deposit within the Eberswalde crater lake (red polygon).

Lastly, the region studied here has remarkable similarities to that of the Jezero crater system. Both Eberswalde and Jezero crater have visibly intact source-to-sink fluvial systems, which is remarkably rare on Mars given the ~3.0 billion years that have elapsed since fluvial processes were pervasive on Mars' surface. Furthermore, both regions have evidence of detrital smectite clays, and indications of a neutral pH environment during the existence of each crater's lake (Goudge et al., 2015b). NASA's Perseverance Rover is to land in Jezero crater in February 2020, with plans to investigate the deltaic deposits there. The results from this study indicating

minimal variability along short reaches of stratal planes may be useful when considering the most economic course as the Perseverance science team explores the delta stratigraphy.

5. Conclusions

We analyzed CRISM spectra from the largest deltaic deposit in Eberswalde crater, the Eberswalde crater watershed, and Northwest Noachis Terra and found evidence of Fe/Mg smectite clays, namely nontronite and saponite, in all regions. The observation of this evidence within Eberswalde crater deposit and within the watershed is a strong indication of a detrital origin for the smectite clays found within the river delta deposit. The presence of detrital smectite clays is indicative of a neutral pH environment during the life of the crater lake within Eberswalde crater, which is an indication that this crater may have been a habitable region previously in Mars' ancient history. Furthermore, our observations indicate the detrital smectite clays may have formed in the subsurface during the Noachian period, which is the time and location thought to be optimal for preserving evidence of past life on Mars. The detrital smectites are sourced from a vast geographic expanse within the watershed, and concentrated in a small rover-accessible locale within Eberswalde crater, making it a compelling site for future missions exploring Mars for evidence of past habitability. And, the results and analyses presented here may provide useful insight and context for comparison to the upcoming NASA Perseverance Rover exploration of the strikingly similar source-to-sink fluvial system at Jezero crater, which also terminates in a deltaic deposit.

References

Ackiss, S., Horgan, B., Seelos, F., Farrand, W., & Wray, J. (2018). Mineralogic evidence for subglacial volcanism in the Sisyphi Montes region of Mars. *Icarus*, *311*, 357-370.

Adler, J. B., Bell III, J. F., Fawdon, P., Davis, J., Warner, N. H., Sefton-Nash, E., & Harrison, T. N. (2019). Hypotheses for the origin of the Hypanis fan-shaped deposit at the edge of the Chryse escarpment, Mars: Is it a delta?. *Icarus*, *319*, 885-908.

Ansan, V., Loizeau, D., Mangold, N., Le Mouélic, S., Carter, J., Poulet, F., ... & Gondet, B. (2011). Stratigraphy, mineralogy, and origin of layered deposits inside Terby crater, Mars. *Icarus*, *211*(1), 273-304.

Arvidson, R. E., Squyres, S. W., Bell, J. F., Catalano, J. G., Clark, B. C., Crumpler, L. S., ... & Gellert, R. (2014). Ancient aqueous environments at Endeavour crater, Mars. *Science*, *343*(6169), 1248097.

Azua-Bustos, A., Fairén, A. G., Silva, C. G., Carrizo, D., Fernández-Martínez, M. Á., Arenas-Fajardo, C., ... & Wierzchos, J. (2020). Inhabited subsurface wet smectites in the hyperarid core of the Atacama Desert as an analog for the search for life on Mars. *Scientific Reports*, *10*(1), 1-17.

Barnhart, C. J., Howard, A. D., & Moore, J. M. (2009). Long-term precipitation and late-stage valley network formation: Landform simulations of Parana Basin, Mars. *Journal of Geophysical Research: Planets*, *114*(E1).

Barnhart, C. J., & Nimmo, F. (2011). Role of impact excavation in distributing clays over Noachian surfaces. *Journal of Geophysical Research: Planets*, *116*(E1).

Bibring, J. P., Langevin, Y., Mustard, J. F., Poulet, F., Arvidson, R., Gendrin, A., ... & Berthe, M. (2006). Global mineralogical and aqueous Mars history derived from OMEGA/Mars Express data. *science*, *312*(5772), 400-404.

Buczkowski, D. L., Seelos, K. D., Murchie, S., Seelos, F., Malaret, E., Hash, C., & CRISM team. (2010a). Extensive phyllosilicate-bearing layer exposed by valley systems in Northwest Noachis Terra. In *Lunar and planetary science conference* (Vol. 41, p. 1458).

Buczkowski, D. L., Murchie, S., Clark, R., Seelos, K., Seelos, F., Malaret, E., & Hash, C. (2010b). Investigation of an Argyre basin ring structure using Mars reconnaissance orbiter/compact reconnaissance imaging spectrometer for Mars. *Journal of Geophysical Research: Planets*, *115*(E12).

Buczkowski, D. L., Seelos, K. D., Murchie, S. L., Seelos, F. P., Malaret, E., & Hash, C. (2013, March). Evidence for multiple widespread buried phyllosilicate-bearing layers between Argyre and Valles Marineris. In *Lunar and Planetary Science Conference* (Vol. 44, p. 2331).

Buczkowski, D., Ackiss, S., Seelos, K., Murchie, S., Seelos, F., Malaret, E., & Hash, C. (2014, April). Her Desher and Nirgal Vallis phyllosilicates: Pedogenesis or groundwater sapping?. In *European Planetary Science Congress* (Vol. 9).

Caudill, C. M. (2020). Characterization of Impactite Clay Minerals with Implications for Mars Geologic Context and Mars Sample Return.

Cockell, C. S., Bush, T., Bryce, C., Direito, S., Fox-Powell, M., Harrison, J. P., ... & Noack, L. (2016). Habitability: a review. *Astrobiology*, *16*(1), 89-117.

Christensen, P. R., Jakosky, B. M., Kieffer, H. H., Malin, M. C., McSween, H. Y., Nealson, K., ... & Ravine, M. (2004). The thermal emission imaging system (THEMIS) for the Mars 2001 Odyssey Mission. *Space Science Reviews*, *110*(1-2), 85-130.

Clark, R. N., & Roush, T. L. (1984). Reflectance spectroscopy: Quantitative analysis techniques for remote sensing applications. *Journal of Geophysical Research: Solid Earth*, *89*(B7), 6329-6340.

Clark, R. N., King, T. V., Klejwa, M., Swayze, G. A., & Vergo, N. (1990). High spectral resolution reflectance spectroscopy of minerals. *Journal of Geophysical Research: Solid Earth*, *95*(B8), 12653-12680.

Davis, J. M., Gupta, S., Balme, M., Grindrod, P. M., Fawdon, P., Dickeson, Z. I., & Williams, R. M. (2019). A diverse array of fluvial depositional systems in Arabia Terra: Evidence for mid-Noachian to early Hesperian rivers on Mars. *Journal of Geophysical Research: Planets*, *124*(7), 1913-1934.

Dehouck, E., Mangold, N., Le Mouélic, S., Ansan, V., & Poulet, F. (2010). Ismenius Cavus, Mars: A deep paleolake with phyllosilicate deposits. *Planetary and Space Science*, *58*(6), 941-946.

DiBiase, R. A., Limaye, A. B., Scheingross, J. S., Fischer, W. W., & Lamb, M. P. (2013). Deltaic deposits at Aeolis Dorsa: Sedimentary evidence for a standing body of water on the northern plains of Mars. *Journal of Geophysical Research: Planets*, *118*(6), 1285-1302.

Ehlmann, B. L., Mustard, J. F., Fassett, C. I., Schon, S. C., Head III, J. W., Des Marais, D. J., ... & Murchie, S. L. (2008). Clay minerals in delta deposits and organic preservation potential on Mars. *Nature Geoscience*, *1*(6), 355-358.

Ehlmann, B. L., Mustard, J. F., Swayze, G. A., Clark, R. N., Bishop, J. L., Poulet, F., ... & Barnouin-Jha, O. (2009). Identification of hydrated silicate minerals on Mars using MRO-CRISM: Geologic context near Nili Fossae and implications for aqueous alteration. *Journal of Geophysical Research: Planets*, *114*(E2).
Ehlmann, B. L., Mustard, J. F., & Murchie, S. L. (2010). Geologic setting of serpentine deposits on Mars. *Geophysical research letters*, *37*(6).
Ehlmann, B. L., Mustard, J. F., Clark, R. N., Swayze, G. A., & Murchie, S. L. (2011a). Evidence for low-grade metamorphism, hydrothermal alteration, and diagenesis on Mars from phyllosilicate mineral assemblages. *Clays and Clay Minerals*, *59*(4), 359-377.
Ehlmann, B. L., Mustard, J. F., Murchie, S. L., Bibring, J. P., Meunier, A., Fraeman, A. A., & Langevin, Y. (2011b). Subsurface water and clay mineral formation during the early history of Mars. *Nature*, *479*(7371), 53-60.
Ehlmann, B. L., Berger, G., Mangold, N., Michalski, J. R., Catling, D. C., Ruff, S. W., ... & Poulet, F. (2013). Geochemical consequences of widespread clay mineral formation in Mars' ancient crust. *Space Science Reviews*, *174*(1-4), 329-364.
Fassett, C. I., & Head III, J. W. (2005). Fluvial sedimentary deposits on Mars: Ancient deltas in a crater lake in the Nili Fossae region. *Geophysical Research Letters*, *32*(14).
Fassett, C. I., & Head III, J. W. (2008). Valley network-fed, open-basin lakes on Mars: Distribution and implications for Noachian surface and subsurface hydrology. *Icarus*, *198*(1), 37-56.
Fassett, C. I. (2016). Ames stereo pipeline-derived digital terrain models of Mercury from MESSENGER stereo imaging. *Planetary and Space Science*, *134*, 19-28.
Fawdon, P., Gupta, S., Davis, J. M., Warner, N. H., Adler, J. B., Balme, M. R., ... & Sefton-Nash, E. (2018). The Hypanis Valles delta: The last highstand of a sea on early Mars?. *Earth and Planetary Science Letters*, *500*, 225-241.
Garzanti, E., Andò, S., & Vezzoli, G. (2008). Settling equivalence of detrital minerals and grain-size dependence of sediment composition. *Earth and Planetary Science Letters*, *273*(1-2), 138-151.
Gibbs, R. J. (1967). The geochemistry of the Amazon River system: Part I. The factors that control the salinity and the composition and concentration of the suspended solids. *Geological Society of America Bulletin*, *78*(10), 1203-1232.
Grant, J. A., & Parker, T. J. (2002). Drainage evolution in the Margaritifer Sinus region, Mars. *Journal of Geophysical Research: Planets*, *107*(E9), 4-1.
Grant, J. A., Golombek, M. P., Wilson, S. A., Farley, K. A., Williford, K. H., & Chen, A. (2018). The science process for selecting the landing site for the 2020 Mars rover. *Planetary and Space Science*, *164*, 106-126.
Goddard, K. (2013). The evolution of sedimentary systems on Mars, and implications for climate in the Hesperian-Amazonian epochs.
Golombek, M. P., Arvidson, R. E., Bell, J. F., Christensen, P. R., Crisp, J. A., Crumpler, L. S., ... & Haldemann, A. F. C. (2005). Assessment of Mars Exploration Rover landing site predictions. *Nature*, *436*(7047), 44-48.
Goudge, T. A., Mustard, J. F., Head, J. W., & Fassett, C. I. (2012). Constraints on the history of open-basin lakes on Mars from the composition and timing of volcanic resurfacing. *Journal of Geophysical Research: Planets*, *117*(E12).
Goudge, T. A., Aureli, K. L., Head, J. W., Fassett, C. I., & Mustard, J. F. (2015a). Classification and analysis of candidate impact crater-hosted closed-basin lakes on Mars. *Icarus*, *260*, 346-367.
Goudge, T. A., Mustard, J. F., Head, J. W., Fassett, C. I., & Wiseman, S. M. (2015b). Assessing the mineralogy of the watershed and fan deposits of the Jezero crater paleolake system, Mars. *Journal of Geophysical Research: Planets*, *120*(4), 775-808.
Grotzinger, J. P., Sumner, D. Y., Kah, L. C., Stack, K., Gupta, S., Edgar, L., ... & Milliken, R. (2014). A habitable fluvio-lacustrine environment at Yellowknife Bay, Gale Crater, Mars. *Science*, *343*(6169), 1242777.
Hayden, A. T., Lamb, M. P., Fischer, W. W., Ewing, R. C., McElroy, B. J., & Williams, R. M. (2019). Formation of sinuous ridges by inversion of river-channel belts in Utah, USA, with implications for Mars. *Icarus*, *332*, 92-110.
Hays, L. E., Graham, H. V., Des Marais, D. J., Hausrath, E. M., Horgan, B., McCollom, T. M., ... & Lynch, K. L. (2017). Biosignature preservation and detection in Mars analog environments. *Astrobiology*, *17*(4), 363-400.
Hoehler, T. M. (2007). An energy balance concept for habitability. *Astrobiology*, *7*(6), 824-838..
Horgan, B. H., Anderson, R. B., Dromart, G., Amador, E. S., & Rice, M. S. (2020). The mineral diversity of Jezero crater: Evidence for possible lacustrine carbonates on Mars. *Icarus*, *339*, 113526.

Hughes, C. M., Cardenas, B. T., Goudge, T. A., & Mohrig, D. (2019). Deltaic deposits indicative of a paleo-coastline at Aeolis Dorsa, Mars. *Icarus*, *317*, 442-453.
Hynek, B. M., & Phillips, R. J. (2003). New data reveal mature, integrated drainage systems on Mars indicative of past precipitation. *Geology*, *31*(9), 757-760.
Irwin III, R. P., & Grant, J. A. (2013). Geologic map of MTM-15027,-20027,-25027, and-25032 quadrangles, Margaritifer Terra region of Mars. *US Geological Survey Scientific Investigations Map*, *3209*.
Irwin III, R. P., Lewis, K. W., Howard, A. D., & Grant, J. A. (2015). Paleohydrology of Eberswalde crater, Mars. *Geomorphology*, *240*, 83-101.
Kokaly, R. F., Clark, R. N., Swayze, G. A., Livo, K. E., Hoefen, T. M., Pearson, N. C., ... & Klein, A. J. (2017). *USGS spectral library version 7* (No. 1035). US Geological Survey.
Krzesinska, A. M., Bultel, B., Viennet, J. C., & Werner, S. C. (2019). Experimental Constraints on the Formation of Vermiculitie, Fe, Mg-Phyllosilicates on Mars with Relevance to the Aqueous History of Oxia Planum. *LPICo*, *2089*, 6216.
Lapôtre, M. G., & Ielpi, A. (2020). The Pace of Fluvial Meanders on Mars and Implications for the Western Delta Deposits of Jezero Crater. *AGU Advances*, *1*(2), e2019AV000141.
Le Deit, L., Flahaut, J., Quantin, C., Hauber, E., Mège, D., Bourgeois, O., ... & Jaumann, R. (2012). Extensive surface pedogenic alteration of the Martian Noachian crust suggested by plateau phyllosilicates around Valles Marineris. *Journal of Geophysical Research: Planets*, *117*(E11).
Loesch, T. N. (2001). Hydrologic Analysis Using GIS. Minnesota GIS/LIS Consortium. In *Spring Workshop, Alexandria, Minnesota, USA*.
Loizeau, D., Mangold, N., Poulet, F., Bibring, J. P., Gendrin, A., Ansan, V., ... & Neukum, G. (2007). Phyllosilicates in the Mawrth Vallis region of Mars. *Journal of Geophysical Research: Planets*, *112*(E8).
Malin, M. C., & Edgett, K. S. (2003). Evidence for persistent flow and aqueous sedimentation on early Mars. *Science*, *302*(5652), 1931-1934.
Malin, M. C., Bell, J. F., Cantor, B. A., Caplinger, M. A., Calvin, W. M., Clancy, R. T., ... & Lee, S. W. (2007). Context camera investigation on board the Mars Reconnaissance Orbiter. *Journal of Geophysical Research: Planets*, *112*(E5).
Maxwell, D. E. (1977). Simple Z model for cratering, ejection, and the overturned flap. In *Impact and explosion cratering: Planetary and terrestrial implications* (pp. 1003-1008).
McEwen, A. S., Eliason, E. M., Bergstrom, J. W., Bridges, N. T., Hansen, C. J., Delamere, W. A., ... & Kirk, R. L. (2007). Mars reconnaissance orbiter's high resolution imaging science experiment (HiRISE). *Journal of Geophysical Research: Planets*, *112*(E5).
McKeown, N., Warner, N. H., Rice, M. S., & Grindrod, P. M. (2013, December). Provenance of the Fluvial-deltaic Sedimentary Deposits Within the Eberswalde Crater Catchment, Mars. In *AGU Fall Meeting Abstracts*.
Meunier, A. (2005). *Clays*. Springer Science & Business Media.
Michalski, J. R., & Niles, P. B. (2010). Deep crustal carbonate rocks exposed by meteor impact on Mars. *Nature Geoscience*, *3*(11), 751-755.
Milliken, R. E., & Bish, D. L. (2010). Sources and sinks of clay minerals on Mars. *Philosophical Magazine*, *90*(17-18), 2293-2308.
Mosser-Ruck, R., Pironon, J., Guillaume, D., & Cathelineau, M. (2003). Experimental alteration of Mg-vermiculite under hydrothermal conditions: formation of mixed-layered saponite-chlorite minerals. *Clay Minerals*, *38*(3), 303-314.
Murchie, S., Arvidson, R., Bedini, P., Beisser, K., Bibring, J. P., Bishop, J., ... & Darlington, E. H. (2007). Compact reconnaissance imaging spectrometer for Mars (CRISM) on Mars reconnaissance orbiter (MRO). *Journal of Geophysical Research: Planets*, *112*(E5).
Mustard, J. F., Murchie, S. L., Pelkey, S. M., Ehlmann, B. L., Milliken, R. E., Grant, J. A., ... & Roach, L. (2008). Hydrated silicate minerals on Mars observed by the Mars Reconnaissance Orbiter CRISM instrument. *Nature*, *454*(7202), 305-309.
Perkins, J. P., Finnegan, N. J., & De Silva, S. L. (2015). Amplification of bedrock canyon incision by wind. *Nature Geoscience*, *8*(4), 305-310.
Pommerol, A., & Schmitt, B. (2008). Strength of the H2O near-infrared absorption bands in hydrated minerals: Effects of measurement geometry. *Journal of Geophysical Research: Planets*, *113*(E12).
Pondrelli, M., Rossi, A. P., Platz, T., Ivanov, A., Marinangeli, L., & Baliva, A. (2011). Geological, geomorphological, facies and allostratigraphic maps of the Eberswalde fan delta. *Planetary and Space Science*, *59*(11-12), 1166-1178.

Poulet, F., Mangold, N., Loizeau, D., Bibring, J. P., Langevin, Y., Michalski, J., & Gondet, B. (2008). Abundance of minerals in the phyllosilicate-rich units on Mars. *Astronomy & Astrophysics*, *487*(2), L41-L44.
Poulet, F., Carter, J., Bishop, J. L., Loizeau, D., & Murchie, S. M. (2014). Mineral abundances at the final four curiosity study sites and implications for their formation. *Icarus*, *231*, 65-76.
Ruff, S. W., Campbell, K. A., Van Kranendonk, M. J., Rice, M. S., & Farmer, J. D. (2020). The case for ancient hot springs in Gusev crater, Mars. *Astrobiology*, *20*(4), 475-499.
Rice, M. S., Gupta, S., Bell III, J. F., & Warner, N. H. (2011). Influence of fault-controlled topography on fluvio-deltaic sedimentary systems in Eberswalde crater, Mars. *Geophysical Research Letters*, *38*(16).
Rice, M. S., Belll III, J. F., Gupta, S., Warner, N. H., Goddard, K., & Anderson, R. B. (2013a). A detailed geologic characterization of Eberswalde crater, Mars. *International Journal of Mars Science and Exploration*, *8*, 15-57.
Rice, M. S., Cloutis, E. A., Bell Iii, J. F., Bish, D. L., Horgan, B. H., Mertzman, S. A., ... & Mountain, B. (2013b). Reflectance spectra diversity of silica-rich materials: Sensitivity to environment and implications for detections on Mars. *Icarus*, *223*(1), 499-533.
Schofield, J. T., Barnes, J. R., Crisp, D., Haberle, R. M., Larsen, S., Magalhaes, J. A., ... & Wilson, G. (1997). The Mars Pathfinder atmospheric structure investigation/meteorology (ASI/MET) experiment. *Science*, *278*(5344), 1752-1758.
Seelos, F. P., Viviano-Beck, C. E., Morgan, M. F., Romeo, G., Aiello, J. J., & Murchie, S. L. (2016). CRISM Hyperspectral Targeted Observation PDS Product Sets—TERs and MTRDRs. *LPI*, (1903), 1783.
Segura, T. L., Toon, O. B., Colaprete, A., & Zahnle, K. (2002). Environmental effects of large impacts on Mars. *Science*, *298*(5600), 1977-1980.
Smith, D. E., Zuber, M. T., Frey, H. V., Garvin, J. B., Head, J. W., Muhleman, D. O., ... & Banerdt, W. B. (2001). Mars Orbiter Laser Altimeter: Experiment summary after the first year of global mapping of Mars. *Journal of Geophysical Research: Planets*, *106*(E10), 23689-23722.
Smith, M. R., Bandfield, J. L., Cloutis, E. A., & Rice, M. S. (2013). Hydrated silica on Mars: Combined analysis with near-infrared and thermal-infrared spectroscopy. *Icarus*, *223*(2), 633-648.
Sun, V. Z., & Milliken, R. E. (2015). Ancient and recent clay formation on Mars as revealed from a global survey of hydrous minerals in crater central peaks. *Journal of Geophysical Research: Planets*, *120*(12), 2293-2332.
Tanaka, K. L. (1997). Sedimentary history and mass flow structures of Chryse and Acidalia Planitiae, Mars. *Journal of Geophysical Research: Planets*, *102*(E2), 4131-4149.
Tarnas, J. D., Mustard, J. F., Lin, H., Goudge, T. A., Amador, E. S., Bramble, M. S., ... & Parente, M. (2019). Orbital identification of hydrated silica in Jezero crater, Mars. *Geophysical Research Letters*, *46*(22), 12771-12782.
Viviano-Beck, C. E., Seelos, F. P., Murchie, S. L., Kahn, E. G., Seelos, K. D., Taylor, H. W., ... & Morgan, M. F. (2014). Revised CRISM spectral parameters and summary products based on the currently detected mineral diversity on Mars. *Journal of Geophysical Research: Planets*, *119*(6), 1403-1431.
Wilson, M. J. (2004). Weathering of the primary rock-forming minerals: processes, products and rates. *Clay Minerals*, *39*(3), 233-266.
Wilson, S. A., Grant, J. A., Howard, A. D., & Buczkowski, D. L. (2018). The nature and origin of deposits in Uzboi Vallis on Mars. *Journal of Geophysical Research: Planets*, *123*(7), 1842-1862.
Weitz, C., Bishop, J., & Grant, J. (2018, September). Analysis of Clay Deposits in and around Ladon Basin. In *European Planetary Science Congress* (Vol. 12).
Wordsworth, R. D. (2016). The climate of early Mars. *Annual Review of Earth and Planetary Sciences*, *44*, 381-408.